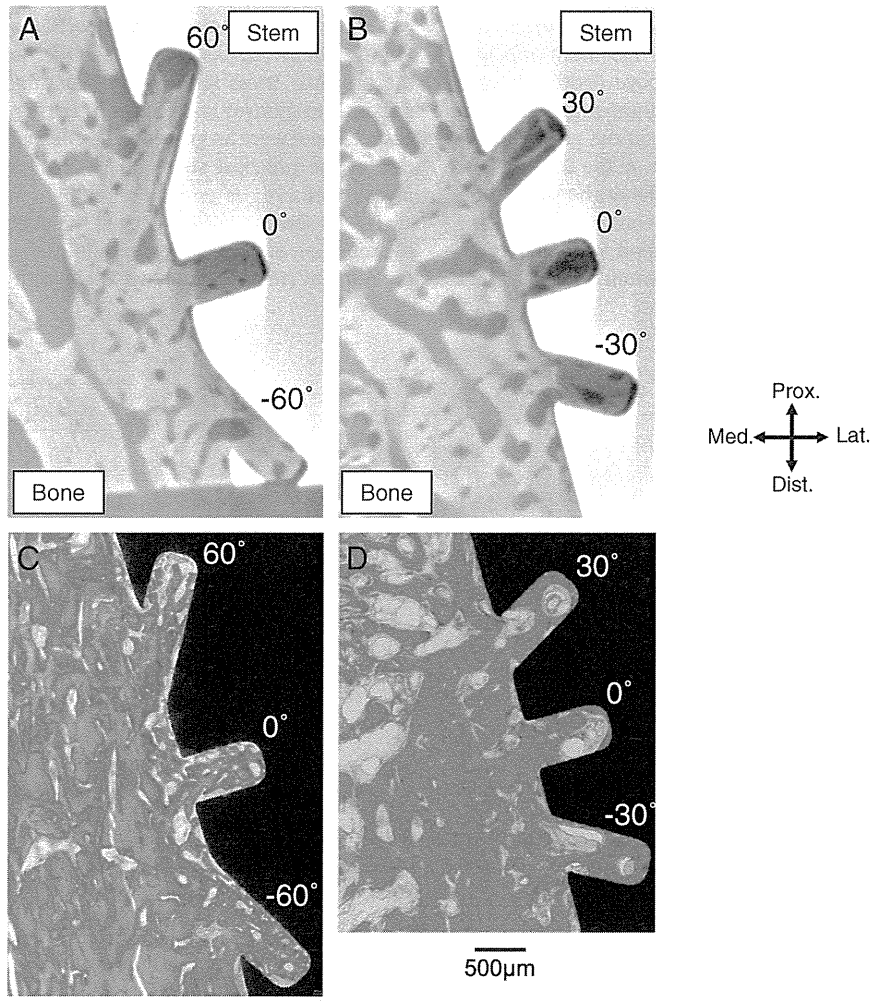

Fig. 4. Bone formation inside the grooves and around the femoral stem in the medial region of the proximal femur 24 weeks after implantation. (A, B) Micro CT images and (C, D) HE staining.

was quantified and categorized into the following ranges: $|\theta| \leq 10°$, $10° < |\theta| \leq 20°$, and $20° < |\theta| \leq 30°$. Particularly in the 60° grooves, the percentage of $|\theta| \leq 30°$ was as high as 80%, and that of $|\theta| \leq 10°$ was also high, revealing that the maximum principal stress was distributed along the direction of the groove depth.

Formation of bone tissue and Col/BAp alignment in the grooves in vivo

Trabecula-like new bone formation was observed in the grooves of all the beagles, as shown in the μCT and HE staining images (Fig. 4). In the 60° grooves, the BV/TV showed the highest value (no statistical significance) and the CV was appreciably small (Table 2), which indicated that high bone mass was achieved homogeneously in the 60° grooves among all 4 of the experimental beagles. In contrast, other grooves showing larger CVs exhibited variable levels of bone mass.

Fig. 5 shows the distributions of the BAp *c*-axis alignment in the grooves. 2D alignment was depicted as the modified elliptical function (Eq. (1)) in a radar diagram (Fig. 5A). The direction of the major axis of the modified ellipse corresponds to the direction of the preferential BAp *c*-axis alignment. The angular difference between groove depth direction and the BAp alignment direction defined by the major axis of the ellipse, and the degree of the BAp alignment along the groove depth direction are summarized in Figs. 5B and C. In the 60° groove, the preferential BAp *c*-axis alignment direction was nearly parallel to the groove depth direction, as indicated by the small angular difference. Moreover, the degree of alignment was highest in the 60° groove. Polarized microscopic imaging (Fig. 6) in the 60° groove showed lamellar bone with highly aligned collagen fibers in the direction of the groove depth (homogeneous bright contrast in Fig. 6C). Osteocytes elongated and aligned along the groove depth direction, indicating the maximum principal stress along the same direction because osteocytes elongate and align in accordance with the direction of applied stress [34]. Conversely, the direction of alignment was dispersed and heterogeneous in the other grooves as represented by bright and dark patches (Figs. 6A and B). Only the 60° groove induced anisotropic bone tissue with a preferential Col/BAp alignment similar to the original trabecular bone.

Table 2
BV/TV inside the grooves introduced in the proximal medial region of the femoral stem.

θ/deg	−60	−30	0	30	60
BV/TV	54.7	52.1	58.7	59.9	66.7
SD	22.6	31.8	18.1	27.1	8.0
CV	41.3	61.0	30.8	45.2	12.0

Discussion

In this study, we have proposed a novel surface morphology design, with oriented grooves in the proximal medial region of the femoral stem, as a new approach to the creation of the artificial hip joints of next generation. When correctly oriented, the grooves allowed the revitalization of Col/BAp alignment and of mechanical function of bone by

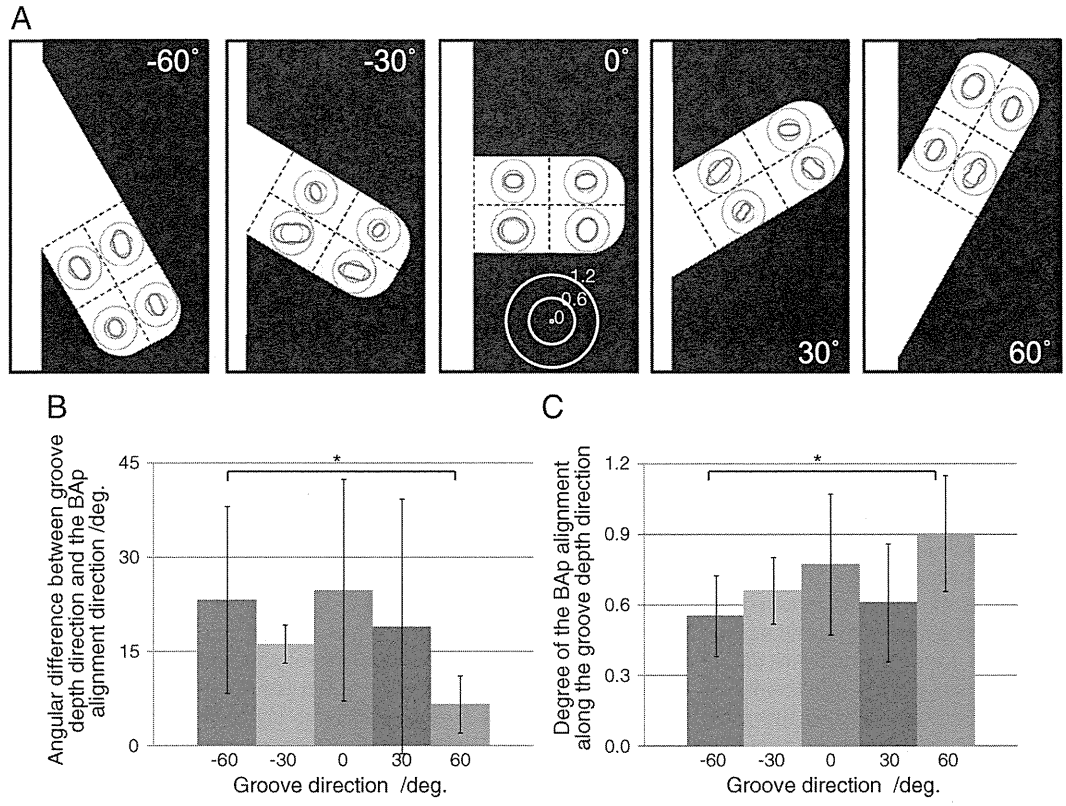

Fig. 5. Distribution of the BAp alignment of the bone formed in the grooves. (A) 2D radar diagrams for the BAp alignment defined by the integrated intensity ratio of (002)/(310) diffraction intensities. (B) Angle between direction of the maximum BAp alignment and the groove depth direction. (C) Degree of BAp alignment to the groove depth direction. *: $P<0.05$.

controlling the stress distribution to the bone. Through an analysis of the maximum principal stress distribution inside the grooves, we examined the optimal angle for oriented grooves and the material property (as YM) of the femoral stem. This implant surface design is a new concept based on the control of the Col/BAp alignment through an active approach from the implant into the bone tissue. Our findings should be important for future implant design guidelines.

Within the grooves introduced at an angle of 60° to the proximal medial surface of the femoral stem, a maximum principal stress distribution along the direction of groove depth was possible (Figs. 2, 3) based on the FEA simulation. Bone ingrowth represented by BV/TV (Table 2) and the preferential Col/BAp alignment (Figs. 5, 6) tended to be enhanced in the 60° groove in which the directions of principal stress and groove depth were almost identical. The findings seem to support the principle that maximum principal stress influences bone ingrowth. The bone formed in the 60° groove might show better mechanical performance than that in the other grooves with relatively weak and more random distribution of BAp alignment because the degree of the BAp *c*-axis alignment is reported to contribute to mechanical function of bone [14].

Principal stress is expected to play a role in regulating Col/BAp alignment in normal cortical bones [8] through an adaptive response

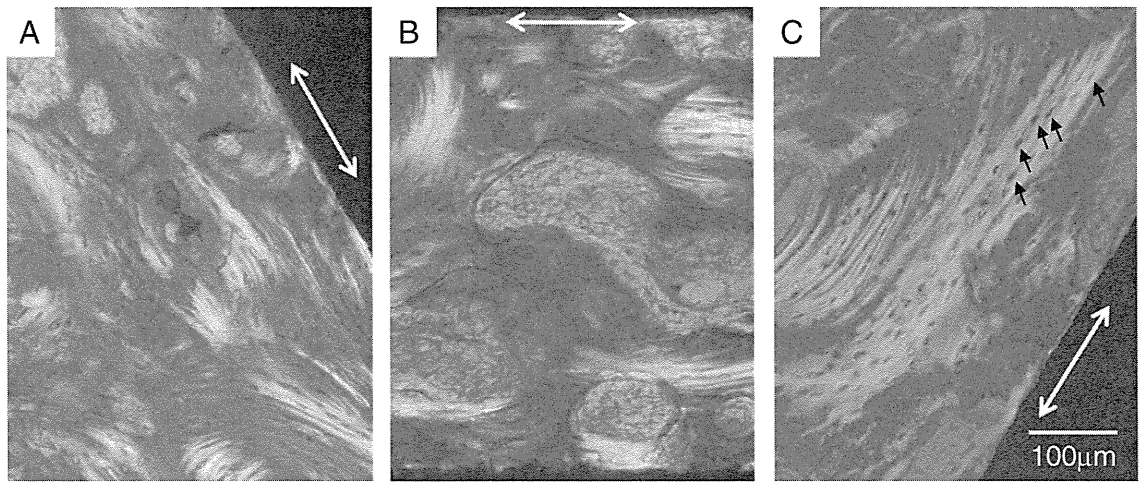

Fig. 6. Polarized microscopy image of the new bone formed in (A) −60° groove, (B) 0° groove and (C) 60° groove. The bright part demonstrates preferential collagen alignment along the groove depth direction indicated by a two-headed arrow. Osteocytes in (C) (black arrow) aligned parallel to the groove depth direction in which the Col/BAp *c*-axis aligned and the maximum principal stress was applied.

of bone which might be mediated by osteocytic mechanosensing [35]. The elongated and aligned osteocytes found in the present study possibly play important roles for the adaptive response to form anisotropic Col/BAp alignment [34]; this needs to be further clarified. Nevertheless, our study is the first to demonstrate that principal stress artificially controlled by a surface morphology-modified implant could also modulate Col/BAp alignment.

In our experiments, only the 60° groove induced an ideal principal stress distribution to produce the resultant anisotropic Col/BAp alignment in the newly formed bone. A characteristic trabecular pattern (secondary compressive group) can be seen at the proximal medial region of the femur, which extends proximally with a high angle that may be close to the grooved angle, despite no quantified data of trabecular angle available. The depth direction of the 60° groove seems to be close to the direction of original trabecula that contacts with the stem used in this study. We thus hypothesize that the association between oriented grooves and trabecular direction is a key factor for achieving appropriate principal stress transfer into the groove.

This hypothesis is supported by the previous studies. Nakano et al. [19] conducted animal tests by introducing implants into a beagle mandible, and determined that unidirectionally oriented through-pores made in the implants were effective for the introduction of new bone with preferred BAp alignment. In the mandible, the bending moment causes principal stress along mesiodistal axis [8,36] in which the Col/BAp and osteon are also aligned [37,38]. This indicates that the desired BAp alignment was promoted because the stress direction on the newly formed bone inside the pores could be maintained normally by unidirectional through-pores oriented parallel to the principal stress, which resulted in a shearing stress increase at the interface between the existing bone and the implant, and the obtainment of a strong binding force [39].

A morphological design of an implant surface should be very effective in providing a normal stress to the bone, in facilitating the optimal BAp alignment of the bone around and inside the implant, and improving bone mechanical function, and, as described, the formation of bone tissue with healthy alignment inside the groove can be expected with a 60° and/or vicinity-angle groove structure examined in this study.

The FEA simulation embeds limitations which should be considered. Only one beagle femur and only one loading condition were used for predicting the maximum principal stress distribution inside the grooves. Moreover, the bone materials were assumed to be homogeneous, while bone tissues have a tremendous degree of heterogeneity in microstructure and properties. While the current simulations showed good agreement with *in vivo* implantation test, the above respects are needed to be taken into account for a more precise optimization of the stem design by FEA.

We used the Ti–6Al–4V implant in our animal models, but we simulated 3 different materials by FEA to estimate the stress distribution. The Ti–6Al–4V alloy is currently the most widely used material for orthopedic implants, and our *in vivo* Ti–6Al–4V implants demonstrated the advantage of the oriented groove on the stem surface on the formation of Col/BAp aligned bone in the groove. However, according to the FEA analysis, the absolute value of the maximum principal stress inside the 60° groove will vary depending on the femoral stem material. The stress value inside the groove elevated with the YM decreased, indicating that the stress shielding inside the grooves is more marked when the femoral stem YM is higher. To inhibit stress shielding, it is preferable that the femoral stem material has a low YM. The β-type titanium (Ti) alloy with low YM is a candidate. The YM of approximately 80 GPa was achieved in a practically-used Ti alloy [40]. Control of the crystallographic texture of the β-type titanium alloy realized even lower YM of about 40 GPa [41,42]. The introduction of an oriented groove structure into a β-type titanium alloy with a low YM can be expected to allow an increase in the stress on the oriented groove, and to improve the Col/BAp alignment more than the Ti–6Al–4V used in the present study.

There are other advantages to the use of femoral stems with lowered YM. For example, in another set of animal experiments using canine femurs, Sumner et al. [43] found that for low YM femoral stems with polyaryletherketone, the amount of bone ingrowth into porous surface layers was significantly higher than that observed with Ti–6Al–4V femoral stems. In addition, they reported that the amount of bone ingrowth into the porous layer, as well as the amount of trabecular bone formed in the marrow cavity, peaked distally near the tip of high YM femoral stems, and that they peaked proximally for low YM femoral stems. Along with the results of this study, this shows that femoral stems with a low YM and a proximal groove structure can promote new bone formation around the femoral stem and inside the grooves. In addition, the application of an optimal stress to the inside of the groove will cause the newly formed bone with preferential Col/BAp alignment, promote load transfer in the proximal portion of the femur, and ultimately achieve good stress transfer to the cortical bone, resulting in the long-term fixation of the implant for bones.

The stem with a rectangular cross-section was used in this study. In the clinical setting, however, a press-fit femoral stems with a round cross-section are also frequently used. The press-fit stem contacts with cortical bone, therefore, the mechanical environment around bone–stem interface may differ from that found in this study. Further study is needed for the surface optimization of the press-fit stem and understanding the formation of the Col/BAp alignment under the cortical bone–stem contact. In addition, the groove size tested in this study was somewhat larger and introduced in a low density when compared with commonly-used porous coatings, because the stem used in this study was designed to understand the optimal groove angle. In terms of the surface effect, finer groove patterning may be beneficial. The effect of groove size should be investigated by a future study.

Most conventional studies on implant optimization have focused on inhibiting the decrease in the stress applied to the existing surrounding bone tissue. In those studies, FEA was used to assess the extent of the decrease in stress applied on the bone around the implant. Conversely, in this study, the ultimate goal was the control of the microstructure of bone materials including the preferred alignment of Col/BAp through positive control of the direction and magnitude of the stress, particularly the maximum principal stress. A healthy microstructure of bone potentially leads to long-term fixation of the implant. Through such an optimal design of new implants using FEA by considering the health of the microstructure of bone, we can expect to achieve next-generation implants with oriented grooves and related implant/bone interface designed to normalize microstructure and function of bone.

Conclusions

In this paper, we proposed a novel artificial hip joint stem with oriented grooves into the proximal medial region of the femoral stem surface, which was expected to control the maximum principal stress distribution and the preferential Col/BAp alignment in the bone formed inside the groove. The FEA and *in vivo* implantation test were performed to examine the advantage of this novel surface modification. The 60° groove toward the proximal side from the normal direction of the stem surface could generate the maximum principal stress along its depth direction and induce new bone with the preferential Col/BAp alignment in the same direction. This seems to support the principle that maximum principal stress influences bone ingrowth including the formation of the Col/BAp alignment. The use of stems with low YM will be able to enhance the principal stress magnitude and resultant formation of the Col/BAp alignment, which may contribute to improvement of the long-term fixation of the implant. The modification of the implant surface morphology considering the health of stress distribution and microstructure of bone is expected to be a novel strategy for future implant design.

Acknowledgments

This work was supported by the Funding Program for Next Generation World-Leading Researchers and Grants-in-Aid for Scientific Research

from the Japan Society for the Promotion of Science (JSPS); the "Super Special Consortia" for supporting the development of cutting-edge medical care (Cabinet Office, Government of Japan; Ministry of Health, Labor and Welfare; Ministry of Education, Culture, Sports, Science, and Technology; and Ministry of Economy, Trade, and Industry); and the Programs of Special Coordination Funds for Promoting Science and Technology from the Ministry of Education, Culture, Sports, Science, and Technology (MEXT) of Japan. The authors thank Mr. N. Nagayama of Industrial Technology Center of Okayama Prefecture and Mr. K. Kuramoto of Nakashima Medical Co., Ltd. for their useful comments.

References

[1] National Hospital Discharge Survey, 2006 annual summary. U.S. Department of Health and Human Services, Center for Disease Control and Prevention, National Center for Health Statistics; 2010.
[2] Saigal A, Fonte M. Solid, shape recovered "bulk" nitinol: part II—mechanical properties. Mater Sci Eng A 2011;528:5551-9.
[3] United States Bone and Joint Decade. Chapter 4: arthritis and related conditions. The burden of musculoskeletal diseases in the United States. Rosemont IL: American Academy of Orthopedic Surgeons; 2011. p. 75–102.
[4] Bozic KJ, Kurtz SM, Lau E, Ong K, Vail TP, Berry DJ. The epidemiology of revision total hip arthroplasty in the United States. J Bone Joint Surg Am 2009;91:128-33.
[5] Tigges S, Stiles RG, Roberson JR. Complications of hip arthroplasty causing periprosthetic radiolucency on plain radiographs. AJR 1994;162:1387-91.
[6] Lindahl H. Epidemiology of periprosthetic femur fracture around a total hip arthroplasty. Injury 2007;38:651-4.
[7] Nakano T, Kaibara K, Ishimoto T, Tabata Y, Umakoshi Y. Biological apatite (BAp) crystallographic orientation and texture as a new index for assessing the microstructure and function of bone regenerated by tissue engineering. Bone 2012;51:741-7.
[8] Nakano T, Kaibara K, Tabata Y, Nagata N, Enomoto S, Marukawa E, Umakoshi Y. Unique alignment and texture of biological apatite crystallites in typical calcified tissues analyzed by microbeam X-ray diffractometer system. Bone 2002;31:479-87.
[9] Viswanath B, Raghavan R, Ramamurty U, Ravishankar N. Mechanical properties and anisotropy in hydroxyapatite single crystals. Scr Mater 2007;57:361-4.
[10] Landis WJ. The strength of a calcified tissue depends in part on the molecular structure and organization of its constituent mineral crystals in their organic matrix. Bone 1995;16:533-44.
[11] Sasaki N, Sudoh Y. X-ray pole figure analysis of apatite crystals and collagen molecules in bone. Calcif Tissue Int 1997;60:361-7.
[12] Bonfield W, Grynpas MD. Anisotropy of the Young's modulus of bone. Nature 1977;270:453-4.
[13] Sasaki N, Ikawa T, Fukuda A. Orientation of mineral in bovine bone and the anisotropic mechanical properties of plexiform bone. J Biomech 1991;24:57-61.
[14] Ishimoto T, Nakano T, Umakoshi Y, Yamamoto M, Tabata Y. Degree of biological apatite c-axis orientation rather than bone mineral density controls mechanical function in bone regenerated using rBMP-2. J Bone Miner Res in press.
[15] Wolff JH. Das gesetz der transformation der knochen. Berlin: Verlag von Augsut Hirschwald; 1892.
[16] Jang IG, Kim IY. Computational study of Wolff's law with trabecular architecture in the human proximal femur using topology optimization. J Biomech 2008;41:2353-61.
[17] Miyabe S, Nakano T, Ishimoto T, Takano N, Adachi T, Iwaki H, Kobayashi A, Takaoka K, Umakoshi Y. Two-dimensional quantitative analysis of preferential alignment of BAp c-axis for isolated human trabecular bone using microbeam X-ray diffractometer with a transmission optical system. Mater Trans 2007;48:343-7.
[18] Rho JY, Roy II ME, Tsui TY, Phar GM. Elastic properties of microstructural components of human bone tissue as measured by nanoindentation. J Biomed Mater Res 1999;45:48-54.
[19] Nakano T, Kan T, Ishimoto T, Ohashi Y, Fujitani W, Umakoshi Y, Hattori T, Higuchi Y, Tane M, Nakajima H. Evaluation of bone quality near metallic implants with and without lotus-type pores for optimal biomaterial design. Mater Trans 2006;47:2233-9.
[20] Huiskes R, Weinans H, Rietbergen BV. The relationship between stress shielding and bone resorption around total hip stems and the effects of flexible materials. Clin Orthop Relat Res 1992;274:124-34.
[21] Engh CA, Bobyn JD, Glassman AH. Porous-coated hip replacement. J Bone Joint Surg Br 1987;69:45-55.
[22] Kim YH, Kim VEM. Uncemented porous-coated anatomic total hip replacement. Int Orthop 1995;19:304-8.
[23] Whiteside LA, White SE, Engh CA, Head W. Mechanical evaluation of cadaver retrieval specimens of cementless bone-ingrown total hip arthroplasty femoral components. J Arthroplast 1993;8:147-55.
[24] Noyama Y, Miura T, Ishimoto T, Itaya T, Niinomi M, Nakano T. Bone loss and reduced bone quality of the human femur after total hip arthroplasty under stress-shielding effects by titanium-based implant. Mater Trans 2012;53:565-70.
[25] Mahaisavariya B, Sitthiseripratip K, Tongdee T, Bohez ELJ, Sloten JV, Oris P. Morphological study of the proximal femur: a new method of geometrical assessment using 3-dimensional reverse engineering. Med Eng Phys 2002;24:617-22.
[26] Huo MH, Martin RP, Zatorski LE, Keggi KJ. Total hip arthroplasty using the Zweymuller stem implanted without cement: a prospective study of consecutive patients with minimum 3-year follow-up period. J Arthroplast 1995;10:793-9.
[27] Sakai R, Sato Y, Itoman M, Mabuchi K. Initial fixation of a finite element model of an AI-Hip cementless stem evaluated by micromotion and stress. J Orthop Sci 2010;10:132-9.
[28] Karageorgiou V, Kaplan D. Porosity of 3D biomaterial scaffolds and osteogenesis. Biomaterials 2005;26:5474-91.
[29] Kuboki Y, Jin Q, Takita H. Geometry of carriers controlling phenotypic expression in BMP-induced osteogenesis and chondrogenesis. J Bone Joint Surg Am 2001;83:105-15.
[30] Rietbergen BV, Müller R, Ulrich D, Rüegsegger P, Huiskes R. Tissue stresses and strain in trabeculae of a canine proximal femur can be quantified from computer reconstructions. J Biomech 1999;32:165-73.
[31] Katti KS. Biomaterials in total joint replacement. Colloids Surf B: Biointerfaces 2004;39:133-42.
[32] O'Grady J, Sheriff M, Likeman P. A finite element analysis of a mandibular canine as a denture abutment. Eur J Prosthodont Restor Dent 1996;4:117-21.
[33] Ishimoto T, Sakamoto T, Nakano T. Orientation of biological apatite in rat calvaria analyzed by microbeam X-ray diffractometer. Mater Sci Forum 2010;638–642:576-81.
[34] Vatsa A, Breuls RG, Semeins CM, Salmon PL, Smit TH, Klein-Nulend J. Osteocyte morphology in fibula and calvaria — is there a role for mechanosensing? Bone 2008;43:452-8.
[35] Burger EH, Klein-Nulend J. Mechanotransduction in bone — role of the lacuno-canalicular network. FASEB J 1999;13:S101-12 [Suppl.].
[36] van Eijden TMGJ. Biomechanics of the mandible. Crit Rev Oral Biol Med 2000;11:123-36.
[37] Nomura T, Gold E, Powers MP, Shingaki S, Katz JL. Micromechanics/structure relationships in the human mandible. Dent Mater 2003;19:167-73.
[38] Bacon GE, Bacon PJ, Griffiths RK. Orientation of apatite crystals in relation to muscle attachment in the mandible. J Biomech 1980;13:725-9.
[39] Alvarez K, Hyun SK, Nakano T, Umakoshi Y, Nakajima H. In vivo osteocompatibility of lotus-type porous nickel-free stainless steel in rats. Mater Sci Eng C 2009;29:1182-90.
[40] Schuh A, Bigoney J, Hönle W, Zeiler G, Holzwarth U, Forst R. Second generation (low modulus) titanium alloys in total hip arthroplasty. Materialwiss Werkstofftech 2007;38:1003-7.
[41] Tane M, Akita S, Nakano T, Hagihara K, Umakoshi Y, Niinomi M, Mori H, Nakajima H. Peculiar elastic behavior of Ti–Nb–Ta–Zr single crystals. Acta Mater 2008;56:2856-63.
[42] Lee SH, Todai M, Tane M, Hagihara K, Nakajima H, Nakano T. Biocompatible low Young's modulus achieved by strong crystallographic elastic anisotropy in Ti–15Mo–5Zr–3Al alloy single crystal. J Mech Behav Biomed Mater 2012;14:48-54.
[43] Sumner DR, Turner TM, Igloria R, Urban RM, Galante JO. Functional adaptation and ingrowth of bone vary as a function of hip implant stiffness. J Biomech 1998;31:909-17.

OPEN

Citation: Cell Death and Disease (2013) 4, e698; doi:10.1038/cddis.2013.226

www.nature.com/cddis

Inhibition of Rac1 promotes BMP-2-induced osteoblastic differentiation

M Onishi[1,2,3], Y Fujita[1,2], H Yoshikawa[3] and T Yamashita*[,1,2]

Small G proteins of the Rho family are pivotal regulators of several signaling networks. The Ras homolog family (Rho) and one of its targets, Rho-associated protein kinase (ROCK), participate in a wide variety of biological processes, including bone formation. A previous study has demonstrated that the ROCK inhibitor Y-27632 enhanced bone formation induced by recombinant human bone morphogenetic protein-2 (BMP-2) *in vivo* and *in vitro*. However, the effect of other Rho family members, such as Ras-related C3 botulinum toxin substrate 1 (Rac1) and cell division cycle 42 (Cdc42), on bone formation remains unknown. In this study, we investigated whether Rac1 also participates in BMP-2-induced osteogenesis. Expression of a dominant-negative mutant of Rac1 enhanced BMP-2-induced osteoblastic differentiation in C2C12 cells, whereas a constitutively active mutant of Rac1 attenuated that effect. Knockdown of T-lymphoma invasion and metastasis 1 (Tiam1), a Rac-specific guanine nucleotide exchange factor, enhanced BMP-2-induced alkaline phosphatase activity. Further, we demonstrated that BMP-2 stimulated Rac1 activity. These results indicate that the activation of Rac1 attenuates osteoblastic differentiation in C2C12 cells.

Cell Death and Disease (2013) **4**, e698; doi:10.1038/cddis.2013.226; published online 27 June 2013
Subject Category: Experimental Medicine

Bone morphogenetic proteins (BMPs) are members of the transforming growth factor-β (TGF-β) superfamily and participate in various processes associated with the differentiation, growth, and death of cells. BMPs were originally identified as inducers of ectopic bone formation, and they are known to have an important role in bone formation and repair.[1,2] BMPs mediate their effects by binding to type I and II serine/threonine kinase receptors, leading to the activation of the intracellular Smad pathway. The binding of BMPs to their receptors induces the phosphorylation of Smads. Phosphorylated Smads then translocate from the cytoplasm to the nucleus to regulate the transcription of various target genes such as *alkaline phosphatase* (*ALP*), *runt-related transcription factor 2* (*Runx2*), and *osteocalcin*.[3]

It has been shown that the function of BMPs is modulated by the small GTPase Ras homolog family A (RhoA) and Rho-associated protein kinase (Rho kinase, ROCK).[4,5] We have shown that the expression of a dominant-negative ROCK mutant in mouse stromal ST2 cells induced osteoblastic differentiation, whereas the expression of a constitutively active ROCK mutant attenuated osteoblastic differentiation.[4] Continuous supply of a specific ROCK inhibitor (Y-27632) enhanced ectopic bone formation induced by BMP-2.[4] Propagating these effects, neogenin acts as a receptor for BMPs and activates RhoA.[5] Knockdown of neogenin in mouse C2C12 myoblasts promoted BMP-2-induced osteoblastic differentiation, whereas overexpression of neogenin suppressed this process.[5] These findings suggest that RhoA–ROCK signaling negatively regulates BMP-induced osteoblastic differentiation.

The Rho family proteins were identified as Ras-like small GTP-binding proteins. Members of the Rho family, including Rho, Rac, and Cdc42, control the assembly and organization of the actin cytoskeleton in mammalian cells.[6] They mediate diverse biological processes, including neuronal morphogenesis, tumor invasion, and bone formation, and act in a coordinated manner to modulate cellular functions.[7,8] However, the effect of Rho family members other than RhoA on osteoblastic differentiation in C2C12 myoblasts remains unclear. In the present study, we assessed the role of Rac1 in BMP-2-induced osteogenesis.

Results

Inhibition of Rac1 promotes BMP-2-dependent osteoblastic differentiation in C2C12 cells. We first examined whether Rac1 activated BMP-2-induced osteoblastic differentiation in C2C12 cells. C2C12 cells were transfected with a dominant-negative mutant of Rac1 (RacDN), a constitutively active mutant of Rac1 (RacCA), or with a control plasmid (mock), with or without rhBMP-2. Thereafter, the cells were stained for ALP (Figure 1a), and the ALP activity was

[1]Department of Molecular Neuroscience, Graduate School of Medicine, Osaka University, Osaka, Japan; [2]JST, CREST, 5, Sanbancho, Tokyo, Japan and [3]Department of Orthopedic Surgery, Graduate School of Medicine, Osaka University, Osaka, Japan
*Corresponding author: T Yamashita, Department of Molecular Neuroscience, Graduate School of Medicine, Osaka University, 2-2 Yamadaoka, Suita-shi, Osaka 565 0871, Japan. Tel: +81 6 68793661; Fax: +81 6 68793669; E-mail: yamashita@molneu.med.osaka-u.ac.jp
Keywords: bone morphogenetic protein; Rac1; C2C12 cells; osteogenesis; Smad signaling
Abbreviations: Rho, Ras homolog family; Rho kinase; ROCK, Rho-associated protein kinase; BMP, bone morphogenetic protein; Rac1, Ras-related C3 botulinum toxin substrate 1; Cdc42, cell division cycle 42; Tiam1, T-lymphoma invasion and metastasis 1; TGF-β, transforming growth factor-β; ALP, alkaline phosphatase; Runx2, runt-related transcription factor 2; RhoA, Ras homolog family A; GEFs, guanine nucleotide exchange factors; Trio, triple functional domain; PAK, p21 protein-activated kinase; JNK, c-Jun N-terminal kinase
Received 13.11.12; revised 27.5.13; accepted 30.5.13; Edited by Y Shi

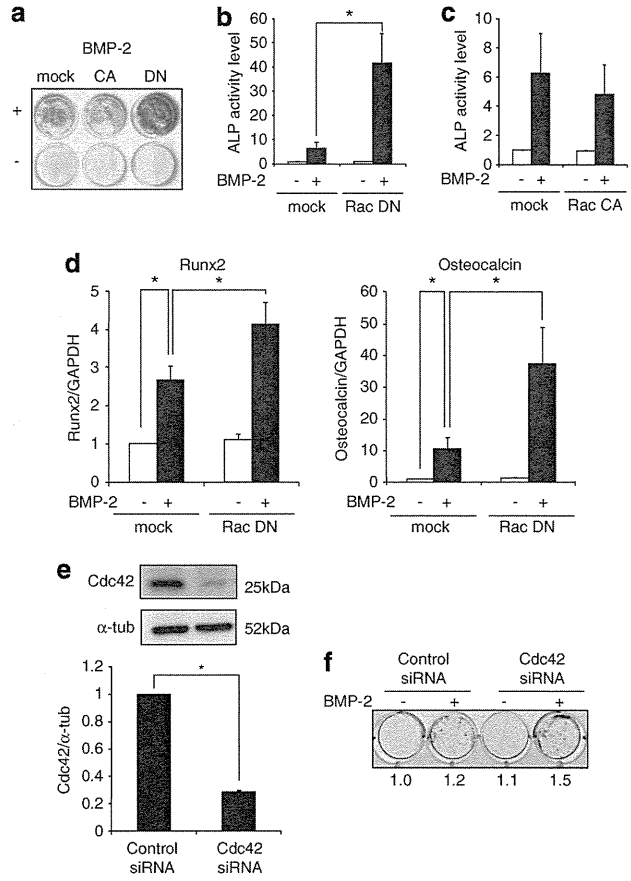

Figure 1 Inhibition of Rac1 promotes BMP-2-induced osteoblastic differentiation. (**a–c**) ALP activity. C2C12 cells were transfected with a dominant-negative form of Rac1 (RacDN), a constitutively active form of Rac1 (RacCA), or with a control plasmid (mock). (**a**) The cells were cultured with or without rhBMP-2 (300 ng/ml) for 2 days and then stained for ALP. (**b**, **c**) Transfected cells were cultured with or without rhBMP-2 (300 ng/ml) for 3 days and then subjected to ALP activity assay. The graphs show fold increase as compared with the levels in the non-treated mock-transfected control group ($n=4$). (**d**) Inhibition of Rac1 promotes BMP-2-induced osteoblast gene expression. C2C12 cells were transfected and treated as in (**a**). mRNA expression of *Runx2* (left graph) and *osteocalcin* (right graph), osteoblastic differentiation markers, was analyzed using real-time PCR. Quantitated mRNA values were normalized to the amount of GAPDH mRNA ($n=5$). (**e**) The effect of Cdc42 siRNA on the expression of Cdc42 in C2C12 cells. Cells were transfected with Cdc42 siRNA or control siRNA for 48 h. Western blots for Cdc42 and α-tubulin are shown (upper 2 panels). The signal intensity was quantified by densitometry and normalized to α-tubulin levels (graph: $n=3$). (**f**) C2C12 cells were transfected with Cdc42 siRNA or control siRNA. The cells were cultured with or without rhBMP-2 (300 ng/ml) for 4 days and then stained for ALP. For (**b–d**): $^*P<0.05$, Tukey–Kramer multiple comparison tests. For (**e**): $^*P<0.05$, unpaired Student's *t* test

quantified (Figures 1b and c). The BMP-2-induced ALP activity was increased in RacDN-transfected cells. Therefore, inhibition of Rac1 promotes BMP-2-induced osteoblastic differentiation in C2C12 cells. The BMP-2-induced ALP activity tended to decrease in RacCA-transfected cells compared with control cells, although we could not find a significant difference ($P>0.05$).

We then examined the expression of two typical osteogenic marker genes—*runt-related transcription factor 2* (*Runx2*) and *osteocalcin*—using real-time PCR. BMP-2 treatment enhanced the expression of *Runx2* and *osteocalcin*, and this increase was significantly higher in cells transfected with RacDN than in mock-transfected plasmids (Figure 1d). These results suggest that Rac1 suppressed BMP-2-induced osteoblastic differentiation in C2C12 cells.

Next, we examined the role of Cdc42, another member of the Rho family of proteins, in BMP-2-induced osteoblastic differentiation. C2C12 cells were transfected with short interfering RNA (siRNA) targeting Cdc42. At 48 h post transfection, we confirmed the knockdown of endogenous Cdc42 in C2C12 cells (Figure 1e). After transfection with Cdc42 siRNA, the cells were treated with or without rhBMP-2, and LP activity was examined. The BMP-2-induced ALP activity was increased in Cdc42 siRNA-transfected cells (Figure 1f). Thus, both Cdc42 and Rac1 negatively regulate BMP-2-induced osteoblastic differentiation in C2C12 cells.

Rac1-GEF mediates the inhibition of BMP-2-induced osteoblastic differentiation. Rho family GTPases are activated through interaction with guanine nucleotide exchange factors (GEFs) that regulate their GTP/GDP exchange. We used the Rac1-specific inhibitor NSC23766, which blocks a subset of Rac1 GEFs, Tiam1, and triple functional domain (Trio).[9] To examine the role of Trio or Tiam1 in C2C12 osteoblastic differentiation induced by BMP-2, we examined the BMP-2-induced ALP activity in these cells. The cells were pre-treated with NSC23766 at 0, 10, or 50 μM and then cultured with rhBMP-2 for 2 days before being subjected to ALP staining (Figure 2a) or 3 days before ALP activity assay (Figure 2b). The BMP-2-induced ALP activities were increased in NSC23766-treated cells in a dose-dependent manner.

Moreover, we examined the expression of *Runx2* and *osteocalcin* in C2C12 cells cultured with rhBMP-2 in the absence or presence of NSC23766 (50 μM) for 2 days (Figure 2c). The expression of these osteogenic marker genes was significantly higher in NSC23766-treated cells in the presence of rhBMP-2. These results suggest that Rac1-GEF, Trio, and Tiam1 can suppress BMP-2-induced osteoblastic differentiation via Rac1 activation.

We also examined whether Rac1 has a role in MC3T3-E1 preosteoblastic cells and primary mesenchymal stem cells derived from rat bone marrow. However, NSC23766 treatment did not promote a BMP-2-dependent increase in ALP activities in MC3T3-E1 cells or mesenchymal stem cells (Figures 2d and e).

Tiam1 regulates BMP-2-induced ALP activity. As the Rac1 inhibitor NSC23766 blocks both Tiam1 and Trio, we performed additional experiments to determine which Rac1-GEF was involved in suppressing BMP-2-induced osteoblastic differentiation. In the first set of experiments, C2C12 cells were transfected with siRNA targeting either Tiam1 or Trio. At 48 h post transfection, we confirmed the knockdown of endogenous Tiam1 or Trio in C2C12 cells (Figures 3a and b). BMP-2-induced ALP activity was significantly higher in the cells transfected with Tiam1 siRNA but not in those transfected with Trio siRNA, as assessed by ALP staining (Figures 3c and e) and ALP quantitative assay (Figures 3d and f). These results demonstrated that Tiam1 but not Trio is

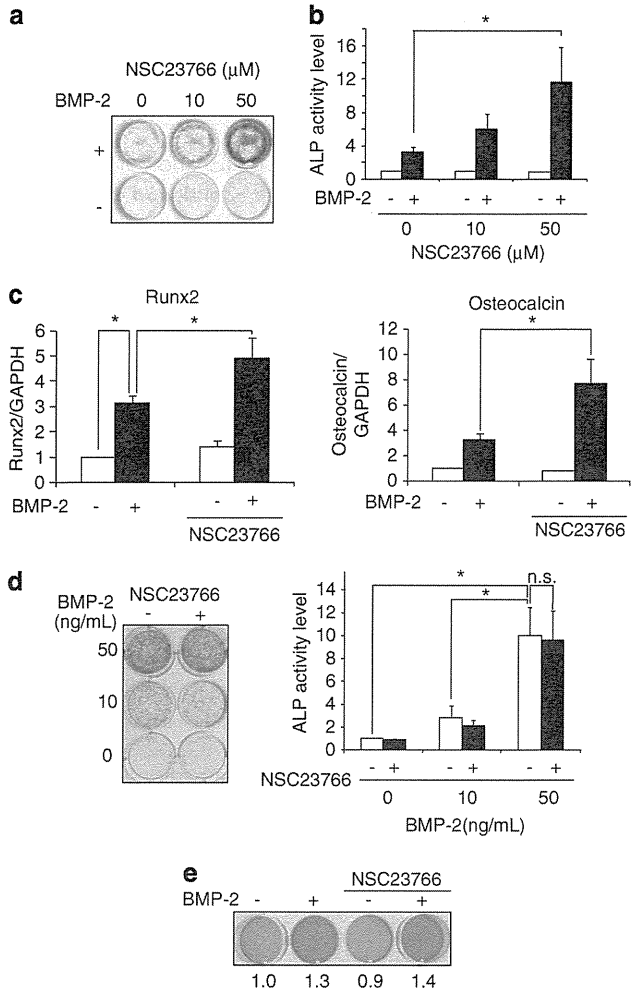

Figure 2 Rac inhibitor enhanced BMP-2-induced osteoblastic differentiation. (**a**, **b**) Rac inhibitor NSC23766 enhanced BMP-2-induced ALP activity. C2C12 cells were pre-treated with NSC23766 (0, 10, and 50 μM) for 12 h and then treated with or without rhBMP-2 (300 ng/ml) for 2 days (**a**) or for 3 days (**b**). ALP activity was detected by cytochemical staining (**a**) or quantified by ALP activity assay (**b**). The graph shows fold increase as compared with the levels in the non-treated control group ($n=5$). (**c**) C2C12 cells were pre-treated with or without NSC23766 (50 μM) for 12 h and then incubated with or without rhBMP-2 (300 ng/ml) for 2 days. mRNA expression of *Runx2* and *osteocalcin* was analyzed as in Figure 1d (left graph: $n=3$; right graph: $n=7$). (**d**) MC3T3-E1 cells were pre-treated with or without NSC23766 (50 μM) and then treated with rhBMP-2 (0, 10, and 50 ng/ml) for 3days. (**e**) Rat Mesenchymal Stem Cells were pre-treated with or without NSC23766 (50 μM) and then treated with rhBMP-2 (300 ng/ml) for 11 days. The cells were subjected to ALP activity assay as described in (**a**) and (**b**). For **b**–**d**: $^*P<0.05$, Tukey–Kramer multiple comparison tests

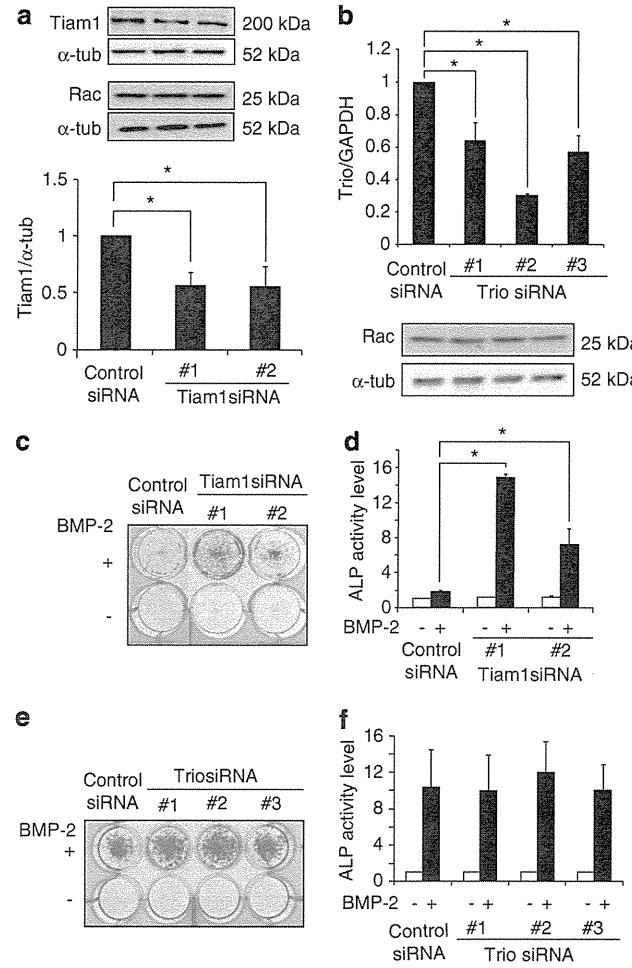

Figure 3 Knockdown of Tiam1 enhances BMP-2-induced ALP activity. (**a**) The effect of Tiam1 siRNA on the expression of Tiam1 in C2C12 cells. Cells were transfected with Tiam1 siRNA or control siRNA for 48 h. Western blots for Tiam1 and α-tubulin are shown (upper two panels). The siRNA did not affect Rac1 expression (lower two panels). The signal intensity was quantified by densitometry and normalized to α-tubulin levels (graph: $n=4$). (**b**) The effect of Trio siRNA on the expression of Trio mRNA in C2C12 cells. C2C12 cells transfected with Trio siRNA or control siRNA were cultured for 48 h, and mRNA expression of Trio was examined. The values are normalized to GAPDH (graph: $n=3$). Trio siRNA did not affect Rac1 expression (lower 2 panels). (**c**, **d**) After Tiam1 siRNA transfection, the cells were cultured with or without BMP-2 (300 ng/ml) for 2 days. (**c**) ALP activity was detected by cytochemical staining. (**d**) ALP activity was analyzed quantitatively. The graph shows fold increase as compared with the levels in cells treated with control siRNA without rhBMP-2 ($n=3$). (**e**, **f**) After Trio siRNA transfection, the cells were cultured with or without rhBMP-2 (300 ng/ml) for 4 days. (**e**) ALP activity was detected by cytochemical staining. (**f**) ALP activity was analyzed quantitatively. The graph shows fold increase as compared with the levels in cells treated with control siRNA without rhBMP-2. For (**a**, **b**, **d**, and **f**): $^*P<0.05$, Tukey–Kramer multiple comparison tests

involved in the suppression of BMP-2-induced ALP activity through Rac1 activation.

BMP-2 induces Rac1 activity in C2C12 cells. Our observation revealed that the inhibition of Rac1 signaling promotes BMP-2-induced osteoblastic differentiation of C2C12 cells.We then examined whether BMP-2 stimulation induced Rac1 activity. We measured the activity of Rac1 by means of a pulldown assay using the GST-fused Rac-binding domain of p21 protein-activated kinase (PAK) beads. Serum-starved C2C12 cells were treated with rhBMP-2 for 1 min. The level of active GTP-bound Rac1 was increased by rhBMP-2 treatment (Figure 4). This result demonstrated that BMP-2 activated Rac1 in C2C12 cells.

Activation of Rac1 does not inhibit Smad signaling. As the activation of Rac1 negatively regulates BMP-2-induced osteoblastic differentiation in C2C12 cells, we next examined

the molecular mechanism underlying the inhibition of BMP signaling by Rac1 activation. BMPs promote bone formation through the activation of Smad signaling.[3] Treatment of rhBMP-2 induces phosphorylation of receptor-activated Smads (Smad1, Smad5, and Smad8; Smad 1/5/8). Phosphorylated Smad 1/5/8 translocates into the nucleus to regulate transcription. To investigate whether the activation of Rac1 inhibited Smad signaling, we analyzed the phosphorylation levels of Smad 1/5/8. Serum-starved C2C12 cells were treated with rhBMP-2 in the absence or presence of NSC23766. However, treatment with NSC23766 did not affect the phosphorylation levels of Smad 1/5/8 (Figure 5a). We further examined the effect of Rac1 on Smad localization. C2C12 cells were transfected with RacDN, cultured with or without rhBMP-2, and subjected to immunofluorescence staining to visualize endogenous Smad1 (Figure 5b). The activation of the BMP pathway leads to accumulation of Smad1 in the nucleus (Figure 5b, left lower 2 panels).[10,11] However, cells transfected with RacDN (arrow) were not affected by the localization of Smad1 (Figure 5b, left lowest panel, arrow). These results indicate that other mechanisms might be involved in the inhibition of osteoblastic differentiation through Rac1 activation.

We further examined whether BMP receptors (BMPRs) were associated with the enhanced ALP activation induced by Rac1 inhibition. C2C12 cells were incubated with a selective inhibitor of BMPR-I, dorsomorphin, for 5 min in the presence or absence of rhBMP-2. rhBMP-2-induced phosphorylation of Smad1/5/8 was inhibited by dorsomorphin (Figure 5c), confirming that dorsomorphin suppresses BMP–Smad signaling. The dorsomorphin treatment did not affect the expression of Rac1 in C2C12 cells (Figure 5d). Enhanced ALP activation induced by Tiam1 siRNA was diminished if the cells were treated with dorsomorphin (Figure 5e). We also demonstrated

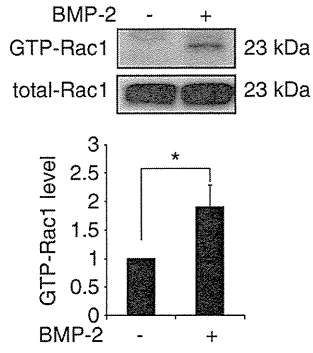

Figure 4 BMP-2 stimulates Rac1 activity in C2C12 cells. BMP-2 activates Rac1 in C2C12 cells. Serum-starved C2C12 cells were treated with or without rhBMP-2 (300 ng/ml) for 1 min and subjected to PAK pulldown assays to detect the active form of Rac (upper panels). Whole-cell lysates were immunoblotted with anti-Rac antibody (lower panels). The relative GTP-Rac1 level was normalized to total Rac1 expression and compared with the level in the cells not treated with rhBMP-2 ($n = 8$). For graph: $^*P < 0.05$, unpaired Student's t test

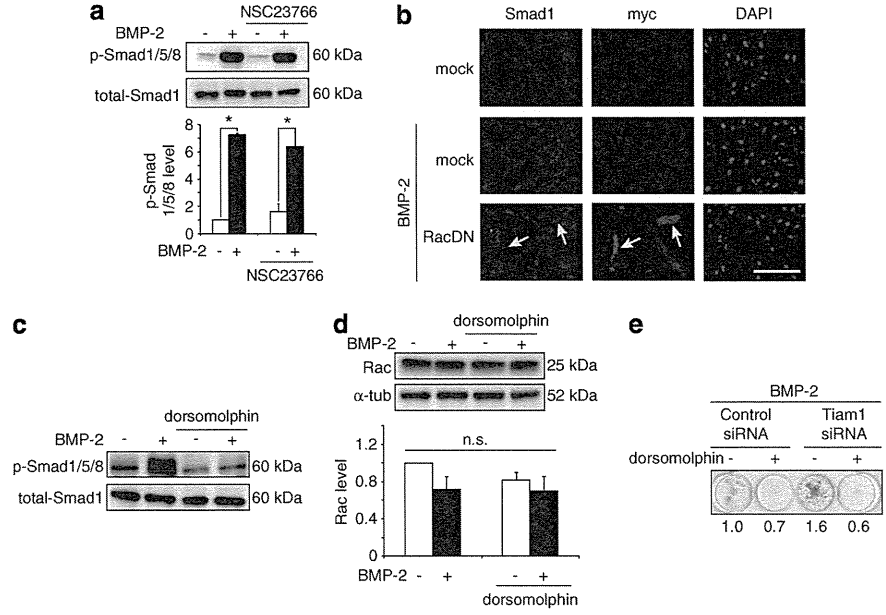

Figure 5 Inhibition of Rac1 does not affect Smad signaling. (**a**) C2C12 cells were pre-treated with NSC23766 as indicated in Figure 2c and then stimulated with or without rhBMP-2 (300 ng/ml) for 15 min. The phosphorylation levels of Smad 1/5/8 were determined by western blotting (panels). The relative phosphorylation levels of Smad 1/5/8 were normalized by total Smad1 level (graph). The graph showed fold increase as compared with the levels in non-treated cells without rhBMP-2 stimulation. In rhBMP-2-stimulated cells, the relative phosphorylation levels of Smad 1/5/8 in the cells pre-treated with or without NSC23766 were not different. For graph: $^*P < 0.05$, Tukey–Kramer multiple comparison tests ($n = 3$). (**b**) C2C12 cells were transfected with a myc-tagged dominant-negative mutant of Rac1 (RacDN) or with control myc (mock) and treated with or without rhBMP-2 (300 ng/ml). After cell fixation and permeabilization, localization of endogenous Smad1 and myc-tagged proteins was detected using an anti-Smad1 antibody (left panels) and an anti-myc antibody (middle panels). Arrows indicate the cells transfected with myc-tagged RacDN. The nuclei were counterstained with DAPI (right panels). The representative images of cells are shown. Scale bar, 200 μM. (**c**) The cells were pre-treated with 3 μM dorsomorphin and were then treated with rhBMP-2 (300 ng/ml) for 5 min. The phosphorylation levels of Smad 1/5/8 were determined by western blotting. Dorsomorphin inhibited BMP-2-induced phosphorylation of Smad 1/5/8. (**d**) Dorsomorphin treatment did not affect the expression level of Rac1. (**e**) Dorsomorphin treatment inhibited the ALP activity induced by Tiam1 siRNA

that the inhibition of Rac1 by itself did not increase the ALP activity in the absence of rhBMP-2 (Figures 1a and 2a). These findings suggest that the BMP–BMPR signal is required for the enhanced ALP activation induced by Rac1 inhibition.

Discussion

In the present study, we assessed the role of Rac1 in osteoblastic differentiation. Inhibition of Rac1 induced the expression of osteoblastic markers such as *ALP*, *Runx2*, and *osteocalcin*. These results indicate that inhibition of Rac1 promotes BMP-2-induced osteoblastic differentiation in C2C12 myoblasts (Figure 6). Although the BMP-2-induced ALP activity was enhanced in RacDN-transfected cells, the ALP activity was not significantly affected by RacCA-transfected cells (Figures 1a–c). The reason why we could not observe significant differences in RacCA-transfected cells could be that the expression of RacCA might not be enough owing to low transfection efficiency. Another possibility is that the activation of Rac1 may only partially inhibit BMP-2-induced osteoblastic differentiation. Rac1 is ubiquitously expressed in most organs and functions to regulate actin cytoskeletal reorganization. Rac1-deficient mice show cell death in numerous locations, particularly in embryonic mesodermal cells.[12] Because of embryonic lethality, the role of Rac1 in developmental bone formation remains largely unknown. Our results provide new leads on the effect of Rac1 on osteoblastic differentiation in C2C12 cells.

Rac1, along with RhoA and Cdc42, is one of the most prominent Rho family GTPases. Rho family GTPases regulate actin cytoskeletal reorganization, cell adhesion, and migration. Therefore, they mediate various biological processes such as neuronal morphogenesis, tumor invasion, and bone formation.[7,8] We have previously shown that neogenin, the newly identified receptor for BMP-2, negatively regulates BMP-2 signal transduction through the activation of RhoA.[5] BMP-2 binding to neogenin activates RhoA and results in the inhibition of osteoblastic differentiation. Inhibition of RhoA promotes BMP-2-induced osteoblastic differentiation and phosphorylation of Smad 1/5/8. Although RhoA regulates Smad signaling to attenuate bone formation, Rac1 did not affect the phosphorylation levels of Smad 1/5/8 (Figure 5). These observations suggest that Rac1 attenuates BMP-2-induced osteoblastic differentiation through a mechanism that is distinct from RhoA.

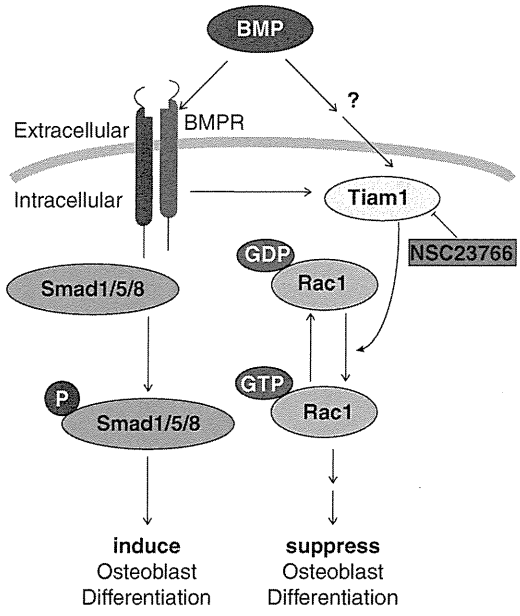

Figure 6 Proposed model of the dual role of BMP signaling in osteoblastic differentiation. BMP-2 induces osteoblastic differentiation through Smad signaling. The present study suggests that BMP-2 suppresses osteoblastic differentiation through Rac1 activation

Our results show that a dominant-negative mutant of Rac1 promotes osteoblastic differentiation in the presence but not in the absence of BMP-2. Therefore, Rac1 possibly mediates osteoblastic differentiation in a BMP-2-dependent manner. We show that treatment of BMP-2 enhances Rac1 activity in C2C12 cells. Our previous study also demonstrated that BMP-2 induced RhoA activity through neogenin and resulted in suppressed osteoblastic differentiation.[5] These findings suggested that BMP-2 not only promotes but also inhibits osteogenesis, although further studies must still be carried out to confirm this. Although it is now possible to generate recombinant human BMPs for medical use, more than 1.5 mg/ml of the recombinant protein is required for bone induction in primates,[13] possibly because of their reduced capability for tissue regeneration.

Inhibition of Rac1 did not promote BMP-2-dependent osteoblastic differentiation in the osteoblast-like MC3T3-E1 cells (Figure 2d). Although the mechanism that explains the discrepancy of the results between C2C12 myoblasts and MC3T3-E1 cells is currently unknown and needs further study, the result supports the hypothesis that the role of Rac1 signaling in osteoblastic differentiation varies depending on the cell types or differentiation stages of osteoblasts.

Rac1 is activated through interaction with the diffuse B-cell lymphoma (Dbl) family GEFs, which regulate the exchange of GDP for GTP.[14] Dbl family GEFs contain the Dbl-homology domain, which is responsible for GEF catalytic activity, and a pleckstrin-homology domain, which is involved in intracellular targeting. Some of the Rho GEFs show activity toward multiple Rho GTPases, whereas others have more restricted specificity. To determine which GEF is responsible for the activation of Rac1 upon BMP stimulation, we used NSC23766, which can effectively inhibit Rac1-GEF, Trio, and Tiam1. Further, we reveal that siRNA-mediated knockdown of Tiam1 but not Trio induced osteoblastic differentiation. These findings suggest that specific Tiam1/Rac1 interaction participates in BMP-2-induced osteoblastic differentiation in C2C12 cells. Tiam1 is a Rac-specific GEF, whereas Trio contains two GEF domains: one N-terminal domain (TrioN), active on RhoG and Rac1,[15] and a C-terminal domain (TrioC), active on RhoA.[16] Different specificity to Rho GTPases is a possible explanation of this effect.

In conclusion, we found that inhibition of Rac1 promoted osteoblastic differentiation upon BMP-2 stimulation. Our results provide evidence that Rac1 and Tiam1 are possible molecular targets for promoting osteogenesis.

Materials and Methods

Antibodies and reagents. The following antibodies were used in this study: mouse monoclonal antibodies to Rac (Upstate, Lake Placid, NY, USA) (1:500) and α-tubulin (Santa Cruz Biotechnology, Santa Cruz, CA, USA) (1:1000); rabbit monoclonal antibodies to Smad1 (Cell Signaling Technology, Beverly, MA, USA) (immunocytochemistry; 1:250, western blotting; 1:1000), phospho-Smad1/5/8 (Cell Signaling Technology) (1:1000), Tiam1 (Santa Cruz Biotechnology) (1:1000), and c-Myc (Santa Cruz Biotechnology) (immunocytochemistry; 1:500, western blotting; 1:1000); and Alexa Fluor 568 anti-rabbit IgG and 488 anti-mouse IgG (Life Technologies, Carlsbad, CA, USA). DAPI was purchased from Dojindo Laboratories (Kumamoto, Japan). The recombinant human bone morphogenetic protein-2 (rhBMP-2) was obtained from R&D Systems (Minneapolis, MN, USA). NSC23766, which is a Rac1-specific inhibitor, was obtained from Merck (Darmstadt, Germany). 5′-Adenosine monophosphate-activated protein kinase inhibitor compound C (Dorsomorphin) was purchased from Calbiochem (San Diego, CA, USA).

Cell culture and transfection. C2C12 cells (Riken BRC Cell Bank, Tsukuba, Japan) were cultured in DMEM with 10% FBS. MC3T3-E1 cells (Riken BRC Cell Bank, Tsukuba, Japan) were cultured in α-minimum essential medium (α-MEM) with 10% FBS and 1% penicillin/streptomycin. Rat primary mesenchymal stem cells (Lonza, Walkersville, MD, USA) were cultured using an R-MSCGMBullet Kit (Lonza).

These cells were transfected using Lipofectamine 2000 (Life Technologies) according to the manufacturer's instructions. The cells were assayed 48 or 72 h after transfection. Myc-tagged mouse Rac1-17N and Rac1-61L were kindly gifted by Dr. A. Hall (Department of Biochemistry and Molecular Biology, University College London, London, UK). siRNA against mouse Cdc42, Tiam1, and Trio was obtained from Life Technologies and contained the following sequences:

Cdc42 (5′-GCAAUGAGUGCUAGUUUUUTT-3′)
Tiam1 no. 1 (5′-UUGAGAAUCUGUUCCUCGGUCCUCC-3′),
Tiam1 no. 2 (5′-UUCUGGAGCUGUCUCAGCACUGCUG-3′),
Trio no. 1 (5′-AUCAUUGGCUCGCUUGGGCACGCUG-3′),
Trio no. 2 (5′-UAAAUAGGAAAUGAGCCUCCUGAGG-3′),
Trio no. 3 (5′-UGCACAUGACUUCUACAGCUUUCUC-3′).

The cells were transfected with 10 nM (Cdc42 siRNA, Tiam1 siRNA no. 1), 2.5 nM (Tiam1 siRNA no. 2), or 30 nM (Trio siRNA no. 1, 2, and 3) siRNA using Lipofectamine RNAi Max (Life Technologies) according to the manufacturer's protocol and cultured for 48 h. Thereafter, the medium was replaced, and the cells were incubated with rhBMP-2 for an additional 48 or 96 h.

Immunocytochemistry. C2C12 cells were fixed with 4% paraformaldehyde for 30 min. The cells were permeabilized, and nonspecific sites were blocked by incubating with blocking solution containing PBS with 0.3% Triton X-100 and 5% BSA. Cells were incubated with the primary antibody diluted in blocking solution for 48 h at 4 °C, washed in PBS, and incubated with Alexa Fluor secondary antibody diluted in blocking solution for 1 h at room temperature. DAPI (1 μg/ml) stain was used to determine nuclear localization. After immunostaining, the slides were mounted with Fluorescent Mounting Medium (DakoCytomation, Glostrup, Denmark).

Assay for Rac activation. After treatment with 300 ng/ml rhBMP-2 or control medium for 1 min, the cells were lysed in a solution containing 25 mM HEPES (pH 7.5), 1% Nonidet P-40, 10 mM $MgCl_2$, 1 mM EDTA, and 1 mM Na_3VO_4. The cell lysates were clarified by centrifugation (20 400 × *g*) at 1 °C for 1 min, and the supernatants were incubated with 50 μg of Rac-binding domain of PAK, which had been freshly coupled with glutathione Sepharose-4B beads (GE Health care, Uppsala, Sweden) at 4 °C for 60 min. The beads were washed four times with lysis buffer and subjected to SDS-PAGE, followed by immunoblotting with anti-Rac1 antibody for active Rac1. The cell lysates were also immunoblotted for total Rac1. The levels of Rac1 activation were calculated by comparing the intensities of the active Rac1 bands with those of the total Rac1 bands in each lane using Image J software (National Institutes of Health). The values obtained were then divided by those of the control, and the data are expressed as fold increase in Rac1 activation over control. The construct for the Rac-binding domain of PAK was kindly gifted by Dr. H. Sumimoto (Department of Molecular and Structural Biology, Kyushu University Graduate School of Medical Science, Fukuoka, Japan).

Real-time PCR. Total RNA was extracted from C2C12 cells using the RNeasy kit (Qiagen, Hilden, Germany) and reverse transcribed using the High-Capacity cDNA Reverse Transcription kit (Applied Biosystems, Foster City, CA, USA). Approximately 4 μg of total RNA was used as a template to synthesize first-strand cDNA. Subsequently, 1 μl of cDNA mixture was used for real-time PCR (total volume, 20 μl) performed using SYBR Green PCR Master Mix (Applied Biosystems) according to the manufacturer's instructions. In addition, the PCR products were purified and sent for sequence analysis using a 7300 Real-time PCR system (Applied Biosystems) to verify amplification of the targeted genes. The optimal conditions were defined as follows: 40 cycles at 50 °C for 2 min, at 95 °C for 10 min, at 95 °C for 15 s, and at 60 °C for 1 min, followed by 1 cycle at 95 °C for 15 s, at 60 °C for 30 s, at 95 °C for 15 s, and at 60 °C for 15 s. The relative mRNA expression of the markers of osteoblastic differentiation was adjusted according to the expression of GAPDH. The primer pairs used for PCR are as follows: *Runx2*, forward 5′-GCTTGATGACTCTAAACCTA-3′, reverse 5′-AAAAAGGGCCCAGTTCTGAA-3′; *Osteocalcin*, forward 5′-CTCACTCTGCTGG CCCTG-3′, reverse 5′-CCGTAGATGCGTTTGTAGGC-3′; Trio forward 5′-GCTG TCACGGCTAGAGGAAC-3′, reverse 5′-CGAGCCTGAGTTCTTTTTGG-3′; and GAPDH, forward 5′-TGAACGGGAAGCTCACTGG-3′, reverse 5′-TCCACCA CCCTGTTGCTGTA-3′. The specificity of each primer set was determined with a pre-test showing amplification of a specific gene by gel visualization and sequencing. The results were analyzed and validated using the relative standard curve method and the delta-delta Ct method.

ALP staining. C2C12 cells were plated on 12-well plates and treated with NSC23766 for 12 h or transfected with the indicated expression vectors for 48 h. The culture medium was replaced with differentiation medium, which was DMEM containing 10% FBS, 10 μg/ml ascorbic acid 2-phosphate (Wako, Osaka, Japan), and 5 mM β-glycerophosphate (Merck KGaA, Darmstadt, Germany) with or without rhBMP-2. The cells were cultured for 2 or 3 days (indicated in the figure legends). MC3T3-E1 cells were plated on 12-well plates and treated with NSC23766 for 12 h. The culture medium was α-MEM containing 10% FBS and 1% penicillin/streptomycin with or without rhBMP-2. The MC3T3-E1 cells were cultured for 3 days. Rat Mesenchymal Stem Cells were plated on 12-well plates and treated with NSC23766 for 12 h. The cells were cultured for 11 days using an R-MSCGMBullet Kit with or without rhBMP-2. These cells were fixed for 15 min with 4% formaldehyde/PBS at room temperature. They were washed with PBS and then stained with nitro blue tetrazolium (NBT; Promega, Madison, WI, USA) and 5-bromo-4-chloro-3-indolyl-phosphate (BCIP; Promega) in ALP buffer (100 mM of Tris-HCl [pH 9.5], 100 mM NaCl, and 5 mM $MgCl_2$).

ALP activity assay. C2C12 cells were plated on 12-well plates and treated with NSC23766 for 12 h or transfected with the indicated expression vectors or siRNA for 48 h. The culture medium was replaced with the differentiation medium described above. Cells were cultured for 2 or 3 days (indicated in the figure legends) and then lysed in Mammalian Protein Extraction Reagent (Thermo Fisher Scientific, Waltham, MA, USA) according to the manufacturer's instructions. ALP activity was assayed using *p*-nitrophenylphosphate as a substrate in the LabAssay ALP (Wako), and the protein content was measured using the bicinchoninic acid (BCA) protein assay kit (Thermo Fisher Scientific).

Western blotting analysis. The siRNA-transfected or rhBMP-2-stimulated C2C12 cells were washed in PBS. After washing the cells, cell lysis was carried out using a lysis buffer containing 50 mM Tris (pH 7.4), 1% Noniet P-40, 150 mM NaCl, and complete Protease Inhibitors (Roche Applied Science, Mannheim, Germany). When we analyzed the phosphorylation levels of Smad 1/5/8, 10 mM NaF and 10 mM Na_3VO_4 were added to the lysis buffer. The proteins were separated by SDS-PAGE followed by immunoblotting.

Statistical analysis. The quantitative data are expressed as mean ± SEM of at least three (indicated in the figure legends when the number was more than three) independent experiments. Statistical analysis of these values was performed using one-way analysis of variance followed by Tukey–Kramer multiple comparison tests or an unpaired Student's *t* test (Figures 1e and 4). *P* values of less than 0.05 were considered significant.

Conflict of Interest

The authors declare no conflict of interest.

Acknowledgements. We thank Dr. A. Hall for providing us plasmids expressing Rac1-17N and Rac1-61L. We are also grateful to Dr. H. Sumimoto for plasmid expressing the Rac-binding domain of PAK.

1. Urist MR. Bone: formation by autoinduction. *Science*, 1965; 150: 893–899.
2. Wozney JM, Rosen V, Celeste AJ, Mitsock LM, Whitters MJ, Kriz RW *et al.* Novel regulators of bone formation: molecular clones and activities. *Science* 1988; **242**: 1528–1534.
3. Miyazono K. A new partner for inhibitory Smads. *Cytokine Growth Factor Rev* 2002; **13**: 7–9.
4. Yoshikawa H, Yoshioka K, Nakase T, Itoh K. Stimulation of ectopic bone formation in response to BMP-2 by Rho kinase inhibitor: a pilot study. *Clin Orthop Relat Res* 2009; **467**: 3087–3095.
5. Hagihara M, Endo M, Hata K, Higuchi C, Takaoka K, Yoshikawa H *et al.* Neogenin, a receptor for bone morphogenetic proteins. *J Biol Chem* 2011; **286**: 5157–5165.
6. Hall A. G proteins and small GTPases: distant relatives keep in touch. *Science* 1998; **280**: 2074–2075.
7. Etienne-Manneville S, Hall A. Rho GTPases in cell biology. *Nature* 2002; **420**: 629–635.
8. Takai Y, Sasaki T, Matozaki T. Small GTP-binding proteins. *Physiol Rev* 2001; **81**: 153–208.
9. Gao Y, Dickerson JB, Guo F, Zheng J, Zheng Y. Rational design and characterization of a Rac GTPase-specific small molecule inhibitor. *Proc Natl Acad Sci USA* 2004; **101**: 7618–7623.
10. Lagna G, Hata A, Hemmati-Brivanlou A, Massague J. Partnership between DPC4 and SMAD proteins in TGF-beta signalling pathways. *Nature* 1996; **383**: 832–836.
11. Liu F, Hata A, Baker JC, Doody J, Carcamo J, Harland RM *et al.* A human Mad protein acting as a BMP-regulated transcriptional activator. *Nature* 1996; **381**: 620–623.
12. Sugihara K, Nakatsuji N, Nakamura K, Nakao K, Hashimoto R, Otani H *et al.* Rac1 is required for the formation of three germ layers during gastrulation. *Oncogene* 1998; **17**: 3427–3433.
13. Govender S, Csimma C, Genant HK, Valentin-Opran A, Amit Y, Arbel R *et al.* Recombinant human bone morphogenetic protein-2 for treatment of open tibial fractures: a prospective, controlled, randomized study of four hundred and fifty patients. *J Bone Joint Surg Am* 2002; **84**: 2123–2134.
14. Zheng Y. Dbl family guanine nucleotide exchange factors. *Trends Biochem Sci* 2001; **26**: 724–732.
15. Blangy A, Vignal E, Schmidt S, Debant A, Gauthier-Rouviere C, Fort P. TrioGEF1 controls Rac- and Cdc42-dependent cell structures through the direct activation of rhoG. *J Cell Sci* 2000; **113**: 729–739.
16. Debant A, Serra-Pages C, Seipel K, O'Brien S, Tang M, Park SH *et al.* The multidomain protein Trio binds the LAR transmembrane tyrosine phosphatase, contains a protein kinase domain, and has separate rac-specific and rho-specific guanine nucleotide exchange factor domains. *Proc Natl Acad Sci USA* 1996; **93**: 5466–5471.

PLOS ONE

Direct Induction of Chondrogenic Cells from Human Dermal Fibroblast Culture by Defined Factors

Hidetatsu Outani[1,2], Minoru Okada[1], Akihiro Yamashita[1], Kanako Nakagawa[2,3], Hideki Yoshikawa[2], Noriyuki Tsumaki[1,2,3]*

1 Department of Cell Growth and Differentiation, Center for iPS Cell Research and Application, Kyoto University, Kyoto, Japan, **2** Department of Orthopaedic Surgery, Osaka University Graduate School of Medicine, Suita, Osaka, Japan, **3** Japan Science and Technology Agency, CREST, Tokyo, Japan

Abstract

The repair of large cartilage defects with hyaline cartilage continues to be a challenging clinical issue. We recently reported that the forced expression of two reprogramming factors (c-Myc and Klf4) and one chondrogenic factor (SOX9) can induce chondrogenic cells from mouse dermal fibroblast culture without going through a pluripotent state. We here generated induced chondrogenic (iChon) cells from human dermal fibroblast (HDF) culture with the same factors. We developed a chondrocyte-specific *COL11A2* promoter/enhancer lentiviral reporter vector to select iChon cells. The human iChon cells expressed marker genes for chondrocytes but not fibroblasts, and were derived from non-chondrogenic *COL11A2*-negative cells. The human iChon cells formed cartilage but not tumors in nude mice. This approach could lead to the preparation of cartilage directly from skin in human, without going through pluripotent stem cells.

Citation: Outani H, Okada M, Yamashita A, Nakagawa K, Yoshikawa H, et al. (2013) Direct Induction of Chondrogenic Cells from Human Dermal Fibroblast Culture by Defined Factors. PLoS ONE 8(10): e77365. doi:10.1371/journal.pone.0077365

Editor: Dimas Tadeu Covas, University of Sao Paulo - USP, Brazil

Received February 20, 2013; **Accepted** September 2, 2013; **Published** October 16, 2013

Funding: This study was supported in part by Scientific Research Grants Nos. 18390415, 19659378 and 21390421 from MEXT and the JST, CREST. The funders had no role in study design, data collection and analysis, decision to publish, or preparation of the manuscript.

Competing Interests: The authors have declared that no competing interests exist.

* E-mail: ntsumaki@cira.kyoto-u.ac.jp

Introduction

Articular cartilage provides shock absorption and lubrication in diarthrodial joints. Articular cartilage is a hyaline cartilage which consists of chondrocytes and cartilage extracellular matrix composed of types II, IX and XI collagen molecules, proteoglycans, and other matrix proteins. Because hyaline cartilage has a poor intrinsic capacity for healing, the loss of cartilage due to trauma or degeneration caused by aging can result in debilitating conditions and osteoarthritis.

Cartilage damage sometimes heals with fibrocartilage, which differs from hyaline cartilage. Fibrocartilage is a type of scar tissue that expresses types I and II collagen; hyaline cartilage, in contrast, does not express type I collagen [1,2]. As the presence of type I collagen impairs the development of cartilage-specific matrix architecture and mechanical function, the repair of cartilage damage by fibrocartilage results in morbidity and functional impairment. Therefore, the goal for repair of cartilage injury is the regeneration of organized hyaline cartilage, rather than healing with fibrocartilage [3]. Although autologous chondrocyte implantation has been successfully performed, the indications are limited to a small size defect, because chondrocytes are limited in number, and because they de-differentiate into fibrochondrocytes during monolayer expansion in culture [4]. Defects larger than 4 cm^2 in size cannot be repaired because of the lack of a sufficient number of bona fide chondrocytes to fill the defect.

Sox9, Sox5 and Sox6 play important roles in the commitment of mesenchymal cells to the chondrocyte lineage. In mouse chimeras, $Sox9^{-/-}$ cells are excluded from the cartilage primordia throughout embryonic development [5,6]. Sox9, Sox5, and Sox6 activate the transcription of chondrocyte-marker genes by binding their enhancers [7–10]. It was reported that the forced expression of Sox5, Sox6 and Sox9 by adenoviral vectors in dermal fibroblasts causes the expression of their target gene, type II collagen [11]. However, the histology of pellet cultures of these cells appears to be fibrocartilaginous, suggesting that the fibroblastic characteristics of the cells persist. Therefore, the cells produced in that study may correspond to fibrocartilaginous cells, rather than hyaline cartilaginous cells. Although dermal fibroblasts represent a readily accessible cell source, their tendency for high expression of type I collagen is a large obstacle to the production of hyaline cartilage. To eliminate the fibroblastic characteristics of these cells, a cell reprogramming process may be necessary.

A large number of autologous hyaline chondrogenic cells may be obtained by generating iPS cells, followed by redifferentiation into a chondrocytic lineage in the future. However, transplantation of redifferentiated chondrocytes is associated with a risk of teratoma formation due to the possible presence of residual undifferentiated cells. Recently, we induced chondrogenic cells directly from adult mouse dermal fibroblast (MDF) culture by transduction of two reprogramming factors (c-Myc, Klf4) and SOX9 [12]. The induced chondrogenic cells formed histologically homogenous hyaline cartilage when injected into the subcutaneous spaces of nude mice. Time-lapse observations of MDF cultures prepared from Nanog-GFP transgenic mice [13] revealed that GFP was not expressed during the induction of chondrogenic cells by transduction of c-Myc, Klf4, and SOX9, proving that the cells do not transition through a pluripotent state during the direct induction of chondrogenic cells from MDFs [14]. Therefore, the

induced chondrogenic cells produced by this method are theoretically free from the risk of teratoma formation.

Future clinical application of this technique of regenerative medicine for articular cartilage diseases will require confirmation that chondrogenic cells can be directly induced from human dermal fibroblast culture. We here generated induced chondrogenic (iChon) cells from human dermal fibroblast (HDF) cultures. We employed nucleofection to misexpress Slc7a1, a receptor for retrovirus, followed by retroviral transduction of the same three factors, to cause the transformation of human dermal fibroblasts into chondrogenic lineage cells. We also developed a chondrocyte-specific *COL11A2* promoter/enhancer lentiviral reporter vector, to select human iChon cells. The human iChon cells expressed type II collagen, but not type I collagen. These human iChon cells generated stable homogenous hyaline cartilage-like tissue without tumor formation for at least 3 months in the subcutaneous spaces of nude mice.

Materials and Methods

Ethics Statement

All experiments were approved by our institutional animal committees, institutional biosafety committees, and institutional review boards of Osaka University and Kyoto University.

Lentiviral Vectors and Transduction

The pLenti6/UbC/mSlc7a1 (Addgene plasmid 17224) was a gift from S. Yamanaka (Center for iPS Cell Research and Application (CiRA), Kyoto University, Kyoto, Japan) [15].

For construction of chondrocyte-specific reporter vectors, the human sequences corresponding to the mouse *Col11a2* promoter and enhancer [16] were amplified by PCR. The human *COL11A2* enhancer was linked to the EGFP-IRES-Puro sequence in the pENTR5′ plasmid (Invitrogen) [12] to prepare pENTR1A-mcs/(EGFP-IresPuro-hInt) (P4-40). The human *COL11A2* promoter was cloned into the pENTR5′ plasmid (Invitrogen) to prepare pENTR5′-mcs/11P (P4-41). The lentiviral vector, pLe6Δ (P4-32) was prepared by deleting the PGKpromoter-EM7-Blastcidine sequence at KpnI sites from pLenti6.4/R4R2/V5-DEST (Invitrogen). pENTR1A-mcs/(EGFP-IresPuro-hInt) (P4-40) was recombined with pENTR5′-mcs/11P (P4-41) and pLe6Δ by the LR clonase II plus reaction (Invitrogen) to prepare pLe6Δ -hLP-mcs/(EGFP-IresPuro-hInt) (P4-42, *COL11a2*-reporter vector), respectively. Lentiviral transduction was performed following the manufacturer's instructions (Invitrogen).

Cell Culture

Human dermal fibroblasts (HDFs) prepared from neonatal foreskin were purchased from Kurabo (KF-4009). On arrival, the HDFs were thawed, and 5×10^5 cell were plated in a 10 cm dish in DMEM supplemented with 10% FBS. The next day, the cells were either untransduced, or were transduced with lentiviral *COL11A2*-reporter vectors overnight. The cells were subsequently split 1:5 into 10 cm dishes and stored in liquid nitrogen until use. Human chondrosarcoma (HCS-2/8) cells were cultured in DMEM supplemented with 10% FBS [17].

Chondrogenically Differentiated Human Bone Marrow Stem Cells

Human bone marrow stem cells (hBMSC) were purchased from Takara (PT-2501). On arrival of frozen stock of hBMSC, the cells were thawed and 3×10^5 cell were plated in a 10 cm dish in αMEM supplemented with 10% FBS. When the cells became confluent, the culture was passaged (P1). Expanded hBMSC (P2) were suspended at 3×10^5 cells/ml in αMEM containing 10% FBS, transferred into a 15-ml tube (Falcon), and centrifuged at 500 g for 5 min. The resulting cell pellet was incubated in a chondrogenic differentiation medium (purchased from Takara [PT-3003, PT-4124]) for 3 weeks, and the resulting cells were called chondrogenically differentiated human bone marrow stem cells (CD-hBMSC).

Nucleofection of *Slc7a1*

The *Slc7a1* sequence from pLenti6/UbC/mSlc7a1 (Addgene plasmid 17224) was cloned into pDONR221 (Invitrogen) by BP clonase (Invitrogen) to prepare pDONR221-mSlc7a1 (P8-63). pDONR221-mSlc7a1 (P8-63) was recombined with pCMVb-gw (P1-32) by the LR reaction (Invitrogen) to prepare pCMV-gw/mSlc7a1 (P9-75). pCMV-gw/mSlc7a1 (P9-75) was introduced into HDFs using nucleofection technology following the manufacturer's instructions (Amaxa).

Retroviral Vectors and Transduction

pMXs-c-MYC (Addgene plasmid 17220) and pMXs-KLF4 (Addgene plasmid 17219), were gifts from S. Yamanaka (Center for iPS Cell Research and Application (CiRA), Kyoto University, Kyoto, Japan) [15]. pMXs-hSOX9 was described previously [12]. Human SOX5 and SOX6 cDNAs were PCR amplified using specific primers (Table S3) and were cloned into pDONR222 vector (Invitrogen) to create pENTR-hSOX5 (P5-41) and pENTR-hSOX6 (P5-42). pENTR-hSOX5 (P5-41) or pENTR-hSOX6 (P5-42) were recombined with pMXs-gw by the LR reaction (Invitrogen) to prepare pMXs-gw/hSOX5 (P8-83) or pMXs-gw/hSOX5 (P8-84). A sequencing analysis showed the hSOX5 and hSOX6 sequences to be correct.

Retroviral transduction was performed as described previously [18]. The Plat-E cells were a gift from T. Kitamura (The Institute of Medical Science, The University of Tokyo, Tokyo, Japan) [19].

Equal amounts of supernatants containing each of the retroviruses were mixed and added to the HDF cultures. After a 16-h incubation in the virus-containing medium, each fibroblast culture in the 10 cm dishes was trypsinized and split 1:5 into new 10 cm dishes in fresh medium (DMEM supplemented with 10% FBS). The medium was changed every other day. In the cultures transduced with lentiviral *COL11A2*-reporter vectors, puromycin was added to the medium when GFP fluorescence was detected in some cells at around 7 days after retroviral transduction. At 21 days after retroviral transduction, dishes were subjected to alcian blue staining. The colony numbers were counted using the NIS Element software program (Nikon). We defined a colony as a cell cluster that was more than 0.5 mm in diameter. Other dishes were used for picking up colonies to generate induced chondrogenic cells.

Alcian Blue Staining

Cells were fixed with methanol at −20°C for 2 min, incubated with 0.1% alcian blue (Sigma) in 0.1 N HCl for 2 h at 25°C, and washed three times with distilled water.

Generation of Induced Chondrogenic Cell Lines

After setting up a sterile cylinder surrounding each colony, we harvested the cells by trypsinization, and replated them in 48 well dishes. After 6–10 days, the cells were replated in 24 well dishes. Then, cells were replated successively into 12 well, 6 well, 6 cm, and 10 cm dishes after culturing for them 3–14 days in each dish. We defined the stage of cells in 10 cm dishes as passage 6. The induced chondrogenic cells were cultured in DMEM containing

10% FBS in the presence of 1 μg/ml puromycin. Induced chondrogenic cells were passaged every 6 days. We initiated the growth curve analyses of induced chondrogenic cells at passage 11.

Genomic PCR Analysis

The iChon cells (passage 11) and HDFs (passage 3) were cultured in 60 mm dishes. After the cells reached confluence, the genomic DNA was extracted and subjected to PCR to amplify transgenes. For the control, a fragment of the GAPDH gene was amplified. The primers used are listed in Table S2.

RT-PCR and Real-time RT-PCR Analyses

After the iChon cells and HDFs cultured in 60 mm dishes reached confluence, the total RNA was extracted using RNeasy Mini Kits (Qiagen). The total RNAs prepared from the redifferentiated human fetal chondrocytes (HFC) were purchased from Cell Applications, Inc. (402RD-R10f). The total RNA was extracted from CD-hBMSCs. The total RNAs were digested with DNase to eliminate any contaminating genomic DNA. For RT-PCR analysis, 1 μg of total RNA was reverse transcribed into first-strand cDNA by using Superscript III Reverse Transcription (Invitrogen). PCR was performed with ExTaq (Takara). The primers used are listed in Tables S2 and S3. For real-time quantitative RT-PCR, 1 μg of total RNA was reverse transcribed into first-strand cDNA by using SuperScript III (Invitrogen) and an oligo$(dT)_{20}$ primer. The PCR amplification occurred in a reaction volume of 20 μl containing 2 μl of cDNA, 10 μl of SYBER PremixExTaq (Takara) and 7900HT (Applied Biosystems). The PCR primers used are listed in Table S3. The RNA expression levels were normalized to the level of *GAPDH* expression.

Determination of Karyotypes

iChon cells were subjected to karyotype analyses at Nihon Gene Laboratories (Japan).

Immunofluorescence Staining

The cells were cultured on culture slides, fixed in 4% paraformaldehyde and permeabilized with 0.5% Tween 20. The cells were then incubated with the primary antibodies listed in Supplemental Table S4. Immune complexes were detected by using the appropriate secondary antibodies conjugated to Alexa Fluor (Table S4).

Bisulfite Genomic Sequencing

Bisulfite treatment was performed by using the EpiTect Bisulfite kit (Qiagen) according to the manufacturer's instructions. The PCR primers used are listed in Table S3. Amplified products were cloned into the pMD20-T vector using a Mighty TA-cloning Kit (Takara). Twelve randomly selected clones were sequenced with the M13 primer, RV, and M13 primer, M4, for each gene.

Pellet Culture

Induced cells were suspended at 5×10^5 cells/ml in DMEM containing 10% FBS, transferred into a 15-ml tube (Falcon), and centrifuged at 500 g for 5 min. The resulting cell pellet was incubated in chondrogenic medium (DMEM, 10% FBS, TGF-β 10ng/ml, DEX 10^{-7} M, Ascorbic acid 50 μg/ml, Pyrubate 100 μg/ml and ITS 6.25 μg/ml) for 3 weeks.

Picrosirius Red Staining and Immunohistochemical Staining

Semi-serial histological sections were stained with picrosirius red using the Picrosisius red stain kit (Plysciences, Inc.) and immunostained with the primary and secondary antibodies listed in Table S4. For controls, sections from osteochodromas obtained at the time of surgery were used to test the anti-type I and anti-type II collagen antibodies.

In vivo Cartilaginous Tissue Formation in Nude Mice

The iChon cells were suspended at 1×10^7 cells/ml in DMEM containing 10% FBS. Then, 100 μl of the cell suspension was injected subcutaneously into the dorsal flank of 6-week-old female nude mice (BALB/cA Jcl-nu/nu). No carrier was used. The mice were sacrificed after 4, 8, 12 weeks, and the injected sites were dissected from the mice. Samples were fixed in 10% neutral buffered formalin, processed, and embedded in paraffin.

Implantation of Human iChon Cells into the Articular Cartilage Defects in Severe Combined Immunodeficiency (SCID) Rats

The skin and joint capsule of a knee joint in 6-week-old SCID rats (F344-Il2rgtm2kyo) [20] were opened. A drill hole with a diameter of 1 mm was created at the femoral groove. A pellet of 5×10^5 iChon cells was implanted into the hole, then the joint capsule and skin were closed. The rats were sacrificed four weeks later.

Culture of iChon Cells Under Osteogenic Conditions

A total of 2×10^5 iChon cells were plated in each well of a six well plate, and cultured in the osteogenic medium (α-MEM supplemented with 10% FBS, 10 mM β-glycerophosphate, 50 μg/ml ascorbic acid, and 10^{-7} M Dexamethasone in the absence or presence of various concentrations of BMP2). The medium was changed every other day. RNAs were extracted from the cells after 21 days of culture, and were subjected to a real-time RT-PCR expression analysis. As control, RNAs were extracted from subchondral bone samples collected from the tibia and femur at the time of surgery.

Implantation of iChon Cells into the Calvarial Defects of SCID Mice

The skin on the head of 5-week-old SCID mice (C.B-17/lcr-scid/scid Jcl) was incised, then a drill hole with a diameter of 1 mm was created at the calvarium. A pellet of 5×10^5 iChon cells was implanted into the hole, then the skin was closed. The mice were sacrificed three weeks later.

Statistical Analysis

The data are shown as averages and standard deviations. Two-tailed Student's *t*-tests were used to compare the data. P values <0.05 were considered to be statistically significant.

Results

The Generation of Human Induced Chondrogenic (iChon) Cells from HDFs by Transduction of c-MYC, KLF4 and SOX9

We first transduced neonatal foreskin HDF cells (Figure 1A, middle left panel) with lentiviral vectors bearing human c-MYC, KLF4 and SOX9, but failed to obtain cells with the polygonal morphology which is typical shape of cultured chondrocytes.

Therefore, we transduced HDFs with these factors following another previously described method using *Slc7a1* encoding a receptor for the retrovirus [15]. We tried to increase the titer of retroviral infection by transducing HDFs with *Slc7a1* using nucleofection technology to increase the expression levels of *Slc7a1*. Two days after the nucleofection of *Slc7a1*, we transduced the HDFs with retroviral c-MYC, KLF4 and SOX9 vectors. Five days after retroviral transduction, we detected polygonal cells in the HDF culture. The polygonal cells (Figure 1A, middle right panel) formed multiple layers at 14 days after transduction, giving rise to cell nodules (Figure 1A, bottom left panel) which is a characteristic of cultured primary chondrocytes [21]. The nodules were surrounded by cells that had the morphological appearance of fibroblasts. These nodules were specifically and intensely stained with alcian blue (Figure 1A, bottom right), suggesting the existence of acid glycosaminoglycans, which is an element of cartilage extracellular matrix. The surrounding cells that had the morphological appearance of fibroblasts were not stained with alcian blue. These results suggest that forced expression of c-MYC, KLF4 and SOX9 can produce induced chondrogenic (iChon) cells from human skin fibroblast cultures.

Selection of Human iChon Cells with a *COL11A2* Enhancer-based Lentiviral Reporter Vector

To remove fibroblastic cells and isolate homogenous polygonal-shaped iChon cell populations, we constructed a chondrocyte-specific reporter vector using EGFP and puromycin-resistant genes linked by the IRES sequence on the lentiviral vector. To obtain chondrocyte-specific expression, we employed promoter and enhancer sequences of the human α2(XI) collagen chain (*COL11A2*) gene (Figure S1A) that correspond to the mouse *Col11a2* promoter and enhancer, which direct chondrocyte-specific expression [16]. The *COL11A2*-reporter vector directed substantial GFP expression in human chondrosarcoma (HCS-2/8) cells [17] but not in HDFs (Figure S1B). We transduced the HDFs with lentiviral *COL11A2*-reporter vectors overnight, split them 1:5, and made a cell stock from these cells. The cell stock of HDFs transduced with reporters was thawed (day 0) and we nucleofected the cells with *Slc7a1* (day 2). We then replated 5×10^5 cells in a 10 cm dish (day 3) and transduced the cells with retroviral vectors bearing c-MYC, KLF4 and SOX9 (day 5) overnight. Immediately after retroviral transduction, the cells were split 1:5 in 10 cm dishes (day 6) (Figure 1B). Polygonal-shaped cells, which appeared 5 days after retroviral transduction with c-MYC, KLF4 and SOX9, started to show *COL11A2-GFP* fluorescence. Subsequently, the polygonal-shaped cells formed nodules. EGFP was expressed in the nodules, but not in the surrounding fibroblastic cells in the absence of puromycin (Figure 1B). The transduction of 5×10^5 HDFs with c-MYC, KLF4 and SOX9 resulted in the formation of 1200 nodules, which showed intense staining for alcian blue in the absence of puromycin (Figure 1C) in five 10 cm dishes. Therefore, the efficiency of the induction of alcian blue-positive cells was 0.24%. On the other hand, the transduction of HDFs with the control retroviral DsRed fluorescent protein vector resulted in neither nodule formation nor substantial alcian blue staining (Figure 1C). Because a combination of SOX9, SOX5 and SOX6 was previously reported to activate the expression of chondrocyte-markers in HDFs [11], we transduced HDFs with SOX9, SOX5 and SOX6. We confirmed that the SOX5, SOX6 and SOX9 proteins were expressed by immunoblot analyses (Figure S2). We found neither nodule formation nor any substantial alcian blue staining in the HDFs transduced with SOX9, SOX5 and SOX6 (Figure 1C). These results indicate that c-MYC and KLF4 play a critical role in the conversion from fibroblasts to chondrogenic cells by SOX9.

To isolate colonies, we started to add puromycin to the medium when GFP fluorescence was detected at 5–7 days after transduction with c-MYC, KLF4 and SOX9. The majority of fibroblastic cells and four-fifths of the polygonal-shaped cells died, leaving 267 surviving colonies, on average, in the culture in the presence of 1 μg/ml puromycin (Figure 1D). On average, 186 out of the 267 colonies were intensely stained with alcian blue and were composed of polygonal cells. The remaining 81 colonies were large and diffuse, as indicated by crystal violet staining, and were composed of fibroblastic cells. The transduction of HDFs with the control retroviral DsRed vector instead of c-MYC, KLF4 and SOX9 vectors produced 107 colonies in the presence of puromycin. These colonies were not stained with alcian blue (Figure 1D), and were composed of fibroblasts. These fibroblasts survived in the presence of puromycin, probably because of the aberrant expression of the lentiviral *COL11A2*-reporter vector. The transduction of HDFs with SOX9, SOX5 and SOX6 also produced 91 colonies in the presence of puromycin. These colonies did not stain for alcian blue (Figure 1D), and were composed of morphologically fibroblastic cells.

Therefore, the transduction of the lentiviral *COL11A2* reporter vector and selection with puromycin resulted in the formation of nodules as colonies, 70% of which were composed of polygonal-shaped cells. The colonies composed of polygonal cells were almost all intensely stained with alcian blue. We picked up colonies which were composed of polygonal-shaped cells, and added them in the wells of 48 well plates and expanded each cell line by replating them onto successively larger dishes. We established 15 clones which reached subconfluency in 10 cm dishes, and were subjected to the further analyses.

Characteristics of the iChon Cells

Isolated human iChon cells showed a polygonal morphology (Figure 2A). We found that all three (c-MYC, KLF4 and SOX9) transgenes were transduced into the genomic DNA (Figure S3A) and were expressed (Figure 2B) in iChon cells. These results suggest that retrovial transgenes were not silenced in iChon cells. A growth curve analysis showed that the proliferation rates of the established human iChon cell lines were lower than those of the parental HDFs (Figure 2C). A karyotype analysis showed that 20 out of 20 cells (iChon 87-18), 20 out of 20 cells (iChon 117-3) and 14 out of 20 cells (iChon 117-37) had normal karyotypes (Figure 2D and Figure S3B).

A real-time RT-PCR analysis showed that human iChon cells expressed neither *COL1A1* nor *COL1A2* mRNAs, which the parental HDFs expressed abundantly (Figure 3A). With regard to the control, redifferentiated human fetal chondrocytes (HFC) expressed both *COL1A1* and *COL1A2*, probably because fibroblasts had contaminated the cells during their collection, or because of dedifferentiation of chondrocytes during culture. On the other hand, the iChon cells expressed chondrocyte-specific marker genes, *COL2A1* and *ACAN*, whereas the HDFs did not. The iChon cell lines showed little expression levels of the hypertrophic chondrocyte marker *COL10A1* and terminally differentiated chondrocyte marker *MMP13* (Figure 3B). Regarding the control, we prepared chondrogenic cells by differentiation from human bone marrow stem cells. Chondrogenically differentiated human bone marrow stem cells (CD-hBMSCs) expressed *COL10A1* and *MMP13*. These expression patterns of iChon cells were maintained after passaging them (Figure S3C).

The bisulfate sequencing analysis revealed that the cytosine guanine (CpG) dinucleotides in the regulatory element of the

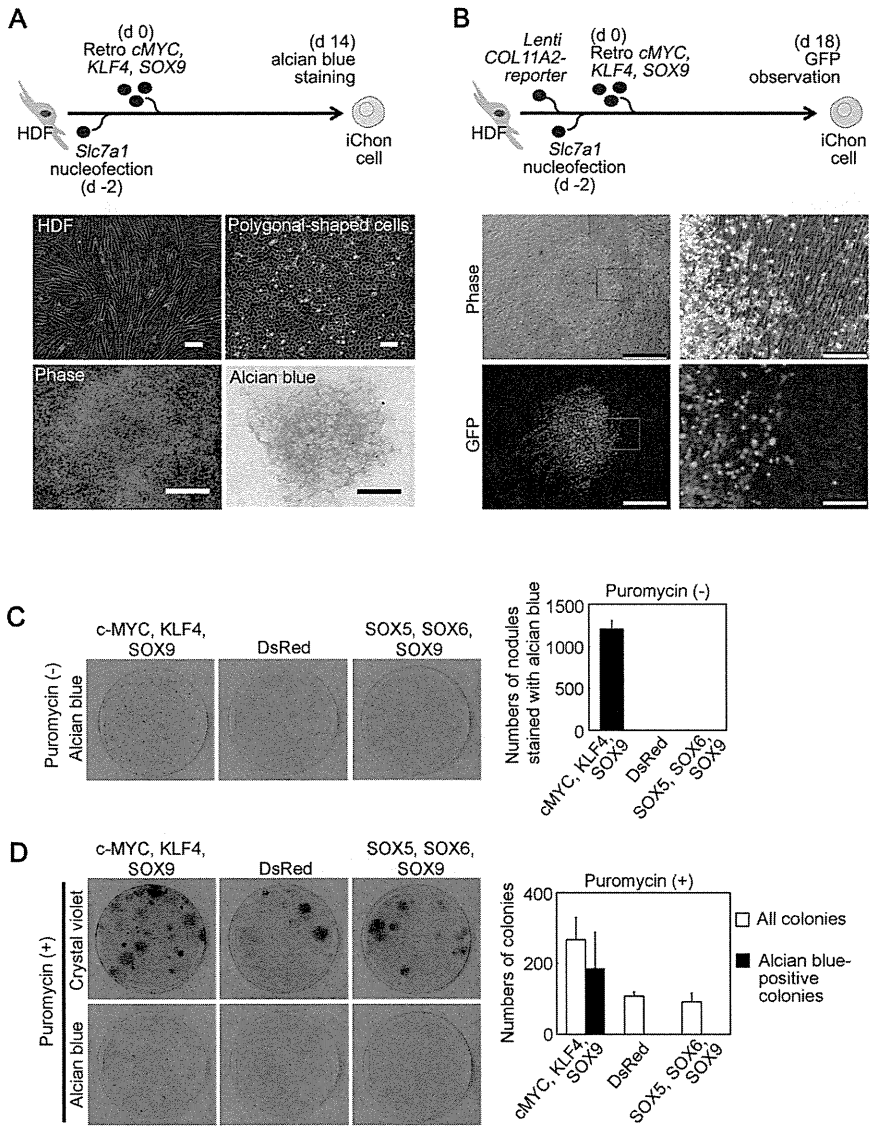

Figure 1. The generation and selection of induced chondrogenic (iChon) cells from human dermal fibroblast (HDF) culture. (**A**) Top, a schematic diagram of the gene transduction. Middle left, HDFs. Middle right, polygonal-shaped cells generated by transduction of c-MYC, KLF4, and SOX9. Bottom left, nodules formed by polygonal-shaped cells. Bottom right, nodules were intensely stained with alcian blue, suggesting the production of glycosaminoglycan. Bars in top panels, 100 μm; Bars in bottom panels, 500 μm. (**B**) Top, a schematic diagram of the gene transduction. Left middle and bottom panels, phase and GFP images of cell nodules formed in HDF culture at 18 days after transduction with c-MYC, KLF4 and SOX9. Right middle and bottom panels, magnification of the boxed region in the left panels. Cells were cultured in the absence of puromycin Bars in left panels, 500 μm; Bars in right panels, 100 μm. (**C**) HDF cultures which had been transduced with lentiviral *COL11A2*- reporter vectors and nucleofected with *Slc7a1* were transduced with retroviral c-MYC, KLF4 and SOX9, or DsRed fluorescent protein, or SOX5, SOX6 and SOX9. Cells were cultured in the absence of puromycin. Dishes (10 cm in diameter) were stained with alcian blue 21 days after retroviral transduction. The numbers of nodules with positive alcian blue staining were counted. (**D**) HDF cultures which had been transduced with lentiviral *COL11A2*- reporter vectors and nucleofected with *Slc7a1* were transduced with retroviral c-MYC, KLF4 and SOX9, or DsRed fluorescent protein, or SOX5, SOX6 and SOX9. Puromycin was added to the medium 7 days after retroviral transduction. Dishes (10 cm in diameter) were stained with crystal violet and alcian blue 21 days after retroviral transduction. The numbers of all colonies stained with crystal violet (white bars) and the numbers of colonies with positive alcian staining (black bars) were counted. In (C and D), after nucleofection of *Slc7a1*, HDFs were replated at a density 5×10^5 cells per 10 cm dish for retroviral transduction. Cells were split 1:5 onto 10 cm dishes immediately after completion of the retroviral transductions. The numbers of nodules in five 10 cm dishes which were derived from one identical dish were added together. Error bars indicate ± SD ($n=3$ dishes).
doi:10.1371/journal.pone.0077365.g001

fibroblast-marker gene *COL1A1* were demethylated in human iChon cells, whereas it was not methylated in the parental HDFs (Figure 3C). These results suggest that the fibroblast marker gene, *COL1A1*, was silenced during the induction of human iChon cells.

We next investigated the cartilage tissue-forming activities of iChon cells by pellet culture. The histology of the pellet culture of iChon cells showed cartilaginous structures (Figure 4A). The matrix of the iChon pellet showed intense metachromatic toluidine blue staining, whereas that of CD-hBMSC pellet looked fibrous. The matrix was hardly formed in the HDF pellet. Picrosirius red staining revealed the fibrous alignment of collagen fibers in CD-hBMSC pellet and HDF pellet, but not in the iChon pellet under polarized microscopic observations. These results suggest that the matrix of the iChon pellet has a hyaline cartilaginous structure;

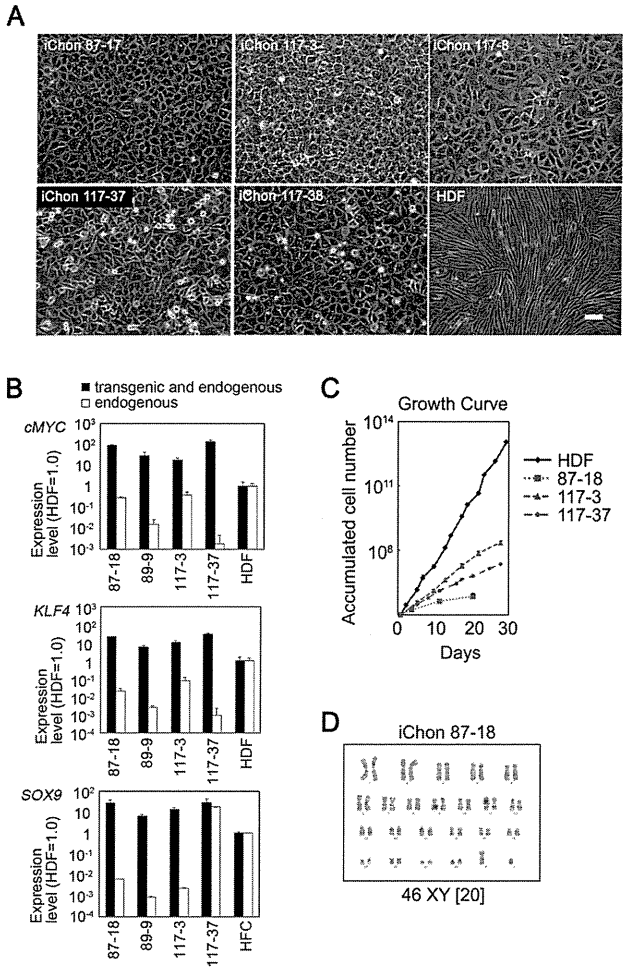

Figure 2. The characteristics of human iChon cell lines. (**A**) Phase images of human iChon cell lines and HDFs. The photos were taken when the cell numbers had expanded and reached 10^7. Bar: 100 μm. (**B**) The mRNA levels of *cMYC*, *KLF4* and *SOX9* in iChon cells. The relative expression levels in comparison to human HDFs or HFCs are shown. The mRNA levels were determined by a real-time RT-PCR analysis using primers specific for endogenous transcripts (white columns) and those common for both transgenic and endogenous transcripts (black columns). The error bars indicate ± SD ($n=3$). (**C**) The growth curves of human iChon cells and parental HDFs. (**D**) The karyotype of human iChon cells. iChon cell line #87-18 was examined at passages 15. A total of 20 cells for each cell line were examined. HDF, human dermal fibroblasts; HFC, redifferentiated human fetal chondrocytes.
doi:10.1371/journal.pone.0077365.g002

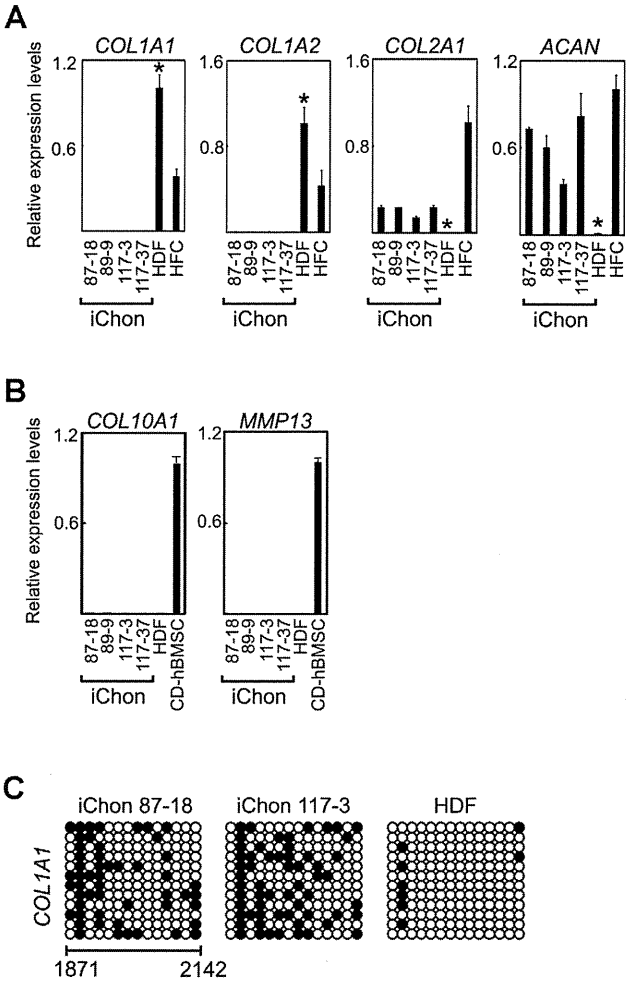

Figure 3. Marker gene expression of human iChon cell lines. RNA samples were extracted from iChon cells at passage 7. (**A**) The quantitative expression analyses of chondrocyte and fibroblast marker genes in human iChon cell lines, HDFs and HFC. Error bars indicate the ± SD ($n=3$). *P<0.01 compared with iChon cell lines by Student's t-test. (**B**) The quantitative expression analyses of chondrocyte hypertrophy and terminal differentiation marker genes in human iChon cell lines, HDFs and CD-hBMSCs. Error bars indicate the ± SD ($n=3$). The relative expression levels of *COL10A1* and *MMP13* mRNAs were zero in iChon cell lines. (**C**) Methylation of the regulartory region of the *COL1A1* gene. Bisulfite genomic sequencing of the regulartory regions of *COL1A1* was performed using DNA derived from iChon cell lines and HDFs. Each horizontal row of circles represents an individual sequencing result from one amplicon. Open circles indicate unmethylated CpG dinucleotides, while closed circles indicate methylated CpGs. The nucleotide numbers for *COL1A1* are indicated at the bottom. The ATG translation initiation codon is set as +1 (GenBank accession number NC 000017, nt 48261457). HDFs, human dermal fibroblasts; HFC, redifferentiated human fetal chondrocytes; CD-hBMSCs, chondrogenically differentiated human bone marrow stem cells.
doi:10.1371/journal.pone.0077365.g003

whereas the matrix of the CD-hBMSC pellet has a fibrocartilaginous structure. Immunohistochemistry showed that the matrix contained type II collagen, but not type I collagen (Figures 4B and 4C). These results suggest that human iChon cells produce hyaline cartilage *in vitro*.

The Origin of Induced Chondrogenic Cells in the HDF Culture

To gain insight into the original cell type which gives rise to chondrogenic cells in HDF culture, we performed time-lapse observations of whole wells of a 6-well plate during the induction of chondrogenic cells (Figure 5). *COL11A2-GFP* fluorescence was not observed at 3 days after retroviral c-MYC, KLF4 and SOX9 transduction throughout the whole wells (Figure 5A, left panel). Some cell clusters expressed *COL11A2-GFP* fluorescence at 8 days after transduction (Figure 5A, second panel, arrowheads), and gradually formed nodules, increasing the level of GFP fluorescence. At 14 days after transduction, some nodules (Figure 5A, third panel, arrowheads) specifically expressed *COL11A2-GFP*, while others did not. We retrospectively analyzed 23 nodules of chondrogenic cells which expressed *COL11A2-GFP* and identified their original cells at the start of induction. The cells of origin of all 23 nodules expressing *COL11A2-GFP* did not express GFP at the start of the induction. A close examination revealed that the cells

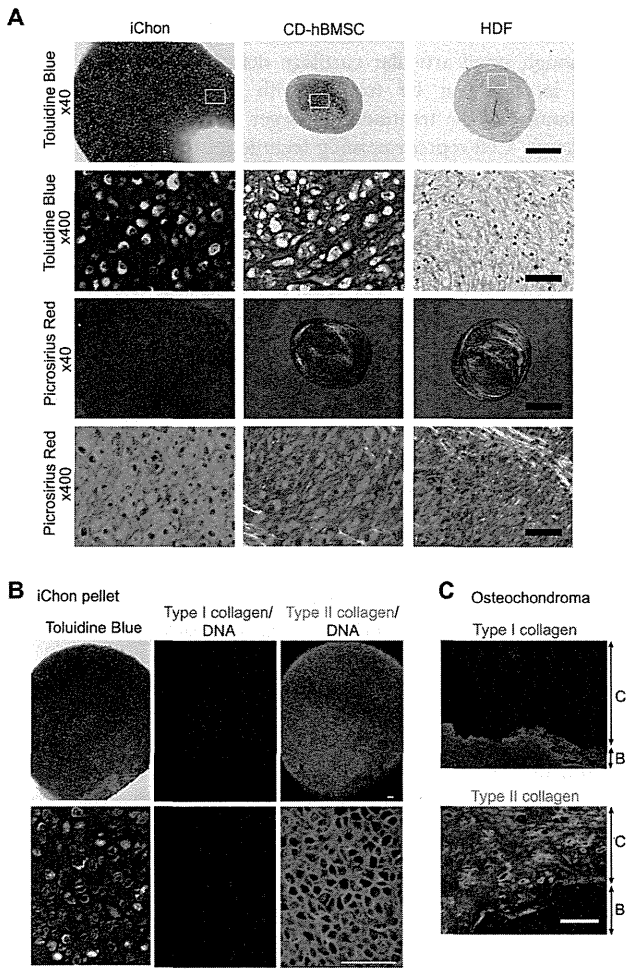

Figure 4. Characterization of matrix of pellet culture of iChon cells. The iChon cells at passage 7 were used. (**A**) After 3 weeks of culture, pellets of iChon cells (# 117-3), chondrogenically differentiated human bone bone marrow stem cells (CD-hBMSC), and human dermal fibroblasts (HDFs) were recovered and processed for histological sections. Semiserial sections were stained with toluidine blue and picrosirius red. Sections stained with picrosirius red were observed under polarized microscopy. Bars in the top and third rows, 500 μm; Bars in the second and bottom rows, 50 μm. (**B**) Semiserial sections of pellets of iChon cells (#117-37) after 3weeks of culture were stained with toluidine blue, and immunostained with anti-type I collagen antibodies and anti-type II collagen antibodies. Bars, 100 μm. (**C**) Control for immunohistological analysis in (B). Histological sections from osteochondroma samples dissected at a time of surgery were immunostained with anti-type I collagen and anti-type II collagen antibodies. Panels are magnification of boxed regions in Figure S7. Bar, 100 μm. *C*, cartilage; *B*, bone.
doi:10.1371/journal.pone.0077365.g004

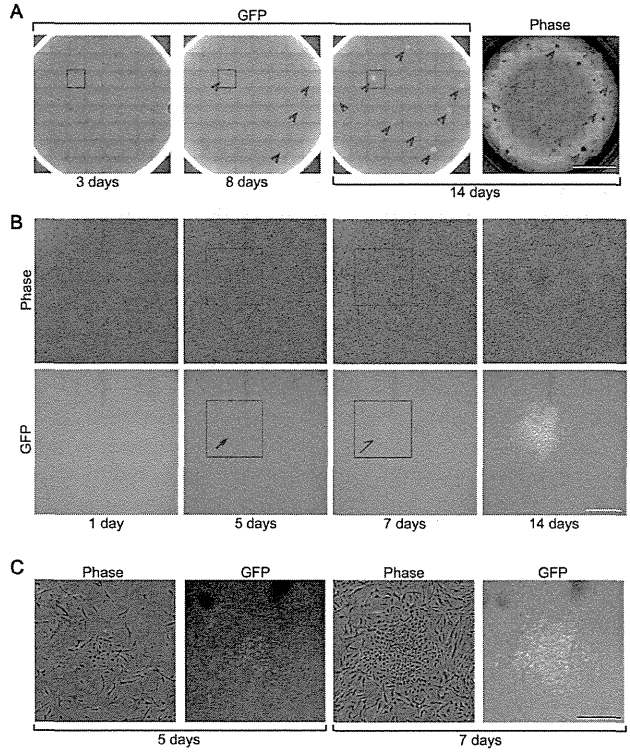

Figure 5. The origins of iChon cells in HDF culture. HDFs were transduced with the lentiviral *COL11A2*-reporter vector, nucleofected with Slc7a1, and transduced with retroviral c-MYC, KLF4 and SOX9 vectors. Cells were replated onto a well of a 6 well plate immediately after completion of the retroviral transduction. The well was cultured in the absence of puromycin and subjected to time-lapse GFP observation using the Biostation CT (Nikon). (**A**) The entire wells were each scanned using a total of 64 images (8 rows×8 columns), and a tiled image was reconstituted. The time-lapse GFP fluorescence of the tiled images at 3, 8 and 14 days after transduction of retroviral c-MYC, KLF4 and SOX9 vectors (3 left panels), and a phase contrast image 14 days after transduction (right panel), spanning an entire well of a 6 well plate are shown. GFP fluorescence was not observed at 3 days after retroviral transduction. Some cell clusters expressed *COL11A2-GFP* fluorescence at 8 days after transduction (arrowheads), and gradually formed nodules, increasing the level of GFP fluorescence. At 14 days after transduction, some nodules (arrowheads) specifically expressed *COL11A2-GFP* and others did not. Bar, 10 mm. (**B**) The magnification of the boxed regions in (A). At 1 day after transduction, no cells expressed *COL11A2-GFP*, suggesting that they were not chondrogenic cells. A cluster of cells with polygonal morphology started to express *COL11A2-GFP* weakly (arrow) at 5 days after transduction. The cells in the cluster increased in number and expressed *COL11A2-GFP* (half-arrow) at 7 days after transduction. A cell cluster formed multiple layers, forming a nodule which expressed *COL11A2-GFP* strongly at 14 days after transduction. These results suggest that iChon cells are derived from non-chondrogenic cells which did not express *COL11A2-GFP*. Bar, 100 μm. (**C**) Magnification of the boxed regions in (B). GFP images were enhanced to detect weak fluorescent signals. Only the polygonal cell clusters expressed *COL11A2-GFP*, but the surrounding fibroblast cells did not express *COL11A2-GFP*. Bar, 50 μm.
doi:10.1371/journal.pone.0077365.g005

from which the *COL11A2-GFP*-positive cells originated did not express *COL11A2-GFP* one day after transduction with c-MYC, KLF4 and SOX9, and only started to express *COL11A2-GFP* at 5–7 days after transduction (Figures 5B and 5C, and Movies S1 and S2). The mouse *Col11a2* regulatory sequences which correspond to the human *COL11A2* promoter-enhancer used in the lentiviral *COL11A2*-reporter gene direct the expression from prechondrogenic cells during mesenchymal condensation [12,16].

In addition, we examined the proportions of cells expressing SOX9 in HDF culture. SOX9 is known to be expressed in chondroprogenitor cells [22]. Immunofluorescence staining of parental HDFs with anti-SOX9 antibodies revealed that the signals were at the background level in almost all cells (Figure S4). The ratio of possible prechondrogenic cells indicated by immunoreactivity against anti-SOX9 antibody in the HDF culture (0.019%, Figure S4C) was lower than the frequency of alcian blue-positive cells generated from HDFs (0.24%, Figure 1D). A close examination revealed that almost all SOX9-positive signals in the

HDF culture were false-positive signals, because the signals were on the edge of cells or debris and did not localize in in the nucleus. These results collectively suggest that non-chondrogenic cells were the major source of the iChon cells.

Hyaline Cartilage Formation by Human iChon Cells in the Subcutaneous Spaces in Nude Mice

We next investigated the cartilage-forming activities of iChon cells *in vivo*. We injected independent iChon cell lines suspended in the medium into the subcutaneous spaces of nude mice (Table S1). Four weeks after injection, we found solid nodules at 14 out of the 42 sites that were injected (33%). We found no nodule formation in the other 28 sites. A histological analysis revealed that these nodules contained cartilage-like tissue (Figure 6A). Cells were scattered in the matrix, which was positively stained with safranin O. We recognized that the cells resided in lacuna, which is characteristic of cartilage histology. An immunohistochemical analysis showed that the matrix contained type II collagen, but not type I collagen, suggesting that the tissue formed by the injection of human iChon cells was hyaline cartilage (Figure 6B). The cells in the cartilage expressed human vimentin, indicating that the injected iChon cells survived and formed cartilage. Longer-term observation showed that the formed cartilage gradually disappeared from the subcutaneous spaces (Table S1). We found no tumor formation at 76 injected sites, including 17 sites that were observed for 3 months (Table S1).

Cartilaginous Tissue Formation by Human iChon Cells in the Articular Cartilage Defects Created in the SCID Rat

We further examined whether iChon cells form cartilage in orthotopic sites. We implanted human iChon cells into defects created in the articular cartilage of six knees of SCID rats. Four weeks after implantation, the defects were partially filled with cartilaginous tissue in four out of the six knees (Figure 6C). The cartilaginous tissues showed positive immunostaining for type II collagen. The expression of type X collagen was below the limit of detection. Immunostaining for human vimentin showed that the cartilaginous tissue was composed of human cells. The human iChon cell-derived cartilaginous tissue was surrounded by scar tissue which consisted of host cells. These results suggest that human iChon cells survive and form cartilaginous tissue in the articular cartilage defects for at least four weeks.

The Low Susceptibility of Human iChon Cells to Osteogenic Conditions

We examined how iChon cells respond to osteogenic conditions. Human iChon cells did not express the OSTEOCALCIN gene (*BGLAP*) or RUNX2 gene when they were cultured in the osteogenic medium containing 100 ng/ml BMP2 for 21 days, although expression of the OSTERIX gene (*SP7*) and the alkaline phosphatase gene (*ALPL*) were slightly increased by the addition of BMP2 (Figure 7A). The *SP7* and *ALPL* genes were expressed in chondrocytes as well as osteoblasts.

Human iChon cells produced cartilaginous tissue and did not form bone, when implanted into the defects created in the calvaria of SCID mice (Figure 7B). The calvarial defects were healed spontaneously, and found to be filled with host bone tissue. These results collectively suggest that human iChon cells did not respond to osteogenic conditions.

Discussion

Although small articular cartilage defects measuring less than 2 cm^2 in size can be treated with autologous chondrocyte transplantation, the treatment of larger cartilage defects remains a challenge. Cell reprogramming techniques have the potential to resolve this problem by providing a sufficient number of hyaline chondrocytes to fill large defects. In this study, we generated human iChon cells directly from HDF culture by transduction of two reprogramming factors (c-MYC and KLF4) and one chondrogenic factor (SOX9). Human iChon cells were generated from non-chondrogenic cells in HDFs, as indicated by the lack of *COL11A2* promoter/enhancer activities and the fact that the majority of the cells had no endogenous SOX9 expression. Human iChon cells generated hyaline cartilage without tumor formation in the subcutaneous space of nude mice. Human iChon cells also formed cartilage in the defects of articular cartilage and did not respond to osteogenic conditions. These results suggest that human iChon cells can be a candidate cell source for regenerative medicine to treat articular cartilage diseases.

It was previously reported that a high level of overexpression of SOX5, SOX6 and SOX9 could activate the expression of chondrocyte-markers in HDFs using adenoviral vectors [11], although fibroblastic characteristics appeared to be remained. We found that the retroviral transduction of c-MYC, KLF4, and SOX9 following *Slc7a1* nucleofection produced substantial numbers of cartilaginous nodules in HDF culture, whereas retroviral transduction of SOX5, SOX6 and SOX9 following *Slc7a1* nucleofection did not. These results indicate that the reprogramming factors c-MYC and KLF4 more efficiently contribute to the SOX9-induced conversion of fibroblasts into chondrogenic cells than SOX5 and SOX6. c-Myc and Klf4 are responsible for erasing the characteristics of fibroblasts during iPS cell induction by c-Myc, Klf4, Oct3/4 and Sox2 [23]. The expression of fibroblast markers was observed to decrease first, followed by an increase in the expression of chondrocyte markers during the induction of mouse chondrogenic cells from MDFs by c-Myc, Klf4 and SOX9 [14]. These findings suggest that c-MYC and KLF4 are involved in epigenetic events in HDFs, and enable SOX9 to direct cells to the chondrogenic lineage during the induction of iChon cells.

The c-MYC, KLF4, and SOX9 transgenes were not silenced in human iChon cells. The silencing of retroviral transgenes is a phenomenon that is a characteristic of pluripotent cells [24] including iPS cells [15]. Retroviral transgenes are not usually silenced in somatic cells and somatic cells which are produced by direct conversion technique [12,25,26]. Human iChon cells expressed neither type X collagen nor MMP13. Human iChon cells retain their chondrogenic phenotype after being passaged in monolayer culture. These results suggest that human iChon cells therefore stay in hyaline chondrocytes and do not undergo hypertrophy. This characteristic of human iChon cells is favorable when considering their application to cell transplantation for the potential treatment of defects of articular cartilage which consists of hyaline cartilage and seldom undergo hypertrophy. CD-hBMSCs tend to undergo hypertrophy and thus can be lost quickly after cell transplantation [27]. Human iChon cells do not undergo hypertrophy, probably because of their continued expression of the SOX9 transgene.

Cell type conversion through iPS cells is associated with two different risks of tumor formation: one is the risk of teratoma formation associated with the pluripotency of iPS cells [28], and the other is associated with the transduction of the reprogramming factors [13]. The iChon cells are theoretically free from the former

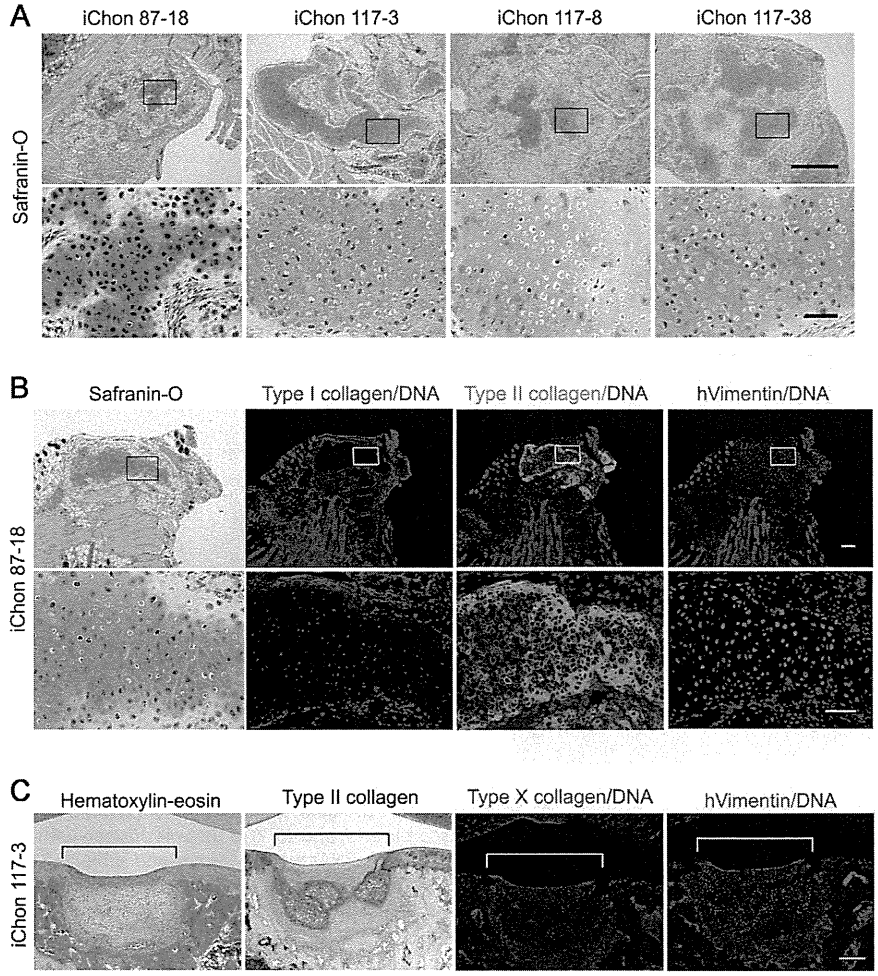

Figure 6. *In vivo* cartilage formation by human iChon cells in the subcutaneous spaces of nude mice (A and B) and articular cartilage defects created in SCID rat (C). The iChon cells at passage 7 were used. Mice were sacrificed at 4 weeks after subcutaneous injection of iChon cells, and nodules at the injected sites were collected. Rats were sacrificed 4 weeks after implantation. (**A**) The histological features of nodules formed by injected iChon cells into subcutaneous spaces of nude mice. Safranin O-fast green-iron hematoxylin staining. Cartilaginous matrix was specifically stained with Safranin O as an orange color. Bars in top panels, 500 μm; Bars in bottom panels, 100 μm. (**B**) The expression of differentiation-related proteins in nodules formed by injected iChon cells into subcutaneous spaces of nude mice. Semiserial sections of nodules derived from injected 87-18 human iChon cell were stained with Safranin O-fast green-iron hematoxylin and immunostained with anti-type I collagen, anti-type II collagen and anti-human vimentin antibodies. The bars in top panels, 500 μm; in bottom panels, 100 μm. (**C**) Human iChon cells (line #117-3) were implanted into defects created in the articular cartilage of the distal femurs of SCID rats. Four weeks after implantation the rats were sacrificed. Semiserial sections were stained with hematoxylin-eosin and immunostained with anti-type II collagen, anti-type X collagen, and anti-human vimentin antibodies. Brackets indicate regions of defects created in the articular cartilage. The bars, 100 μm.
doi:10.1371/journal.pone.0077365.g006

risk, because mouse iChon cells do not enter a pluripotent state during induction, as indicated by the lack of Nanog-GFP expression during induction [14]. However, iChon cells are obviously still associated with the latter risk, because c-MYC and KLF4 are used, although the human iChon cells did not produce tumors for at least 3 months after being injected into nude mice. Safer iPS cells have recently been generated by using integration-free vectors such as episomal plasmid vectors [29] and Sendi virus vectors [30]. Because persistent transgene expression is not necessary for the maintenance of mouse iChon cells as long as they are cultured in a chondrogenic medium containing TGF-β and BMPs [12], it will be ideal to generate human iChon cells by transient expression of c-MYC and KLF4 using integration-free vectors, to minimize the risk of tumor formation. The persistent expression of the SOX9 transgene may positively contribute to the stable chondrogenic phenotype of iChon cells without undergoing hypertrophy in this study. If iChon cells are generated by the transient expression of c-MYC, KLF4 and SOX9, such iChon cells would undergo hypertrophy in a manner similar to that of CD-hBMSCs. An engineered cartilage using CD-hBMSCs undergo hypertrophy faster than articular cartilage and thus can be lost quickly after cell transplantation [27]. However, the constitutive expression of Sox9 can be of another concern, because all tissues undergo remodeling *in vivo*, and an engineered cartilage that does not respond to physiological regulation may present long-term challenges. Further study will thus be needed to stringently control the hypertrophy of such iChon cells during cartilage repair.

Human iChon cells differ from mouse induced chondrogenic cells in several aspects. The karyotypes of the majority of human iChon cells were normal, whereas the karyotypes are fairly unstable in mouse iChon cells [12]. Human iChon cell lines did